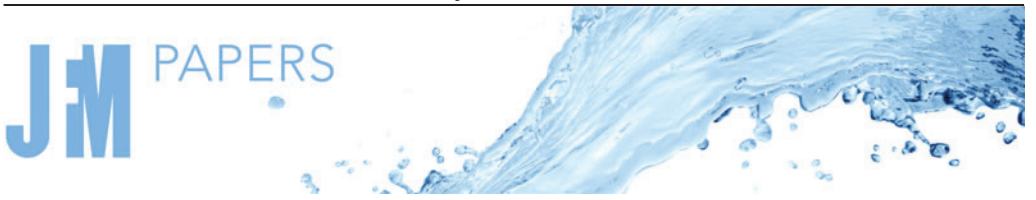
J. Fluid Mech. (2022), *vol*. 947, A42, doi:10.1017/jfm.2022.688



Prediction of triple point trajectory on two-dimensional unsteady shock reflection over single surfaces

He Wang[1], **Zhigang Zhai**[1,†] **and Xisheng Luo**[1]

[1]Advanced Propulsion Laboratory, Department of Modern Mechanics, University of Science and Technology of China, Hefei 230026, PR China

(Received 15 March 2022; revised 20 June 2022; accepted 5 August 2022)

The two-dimensional (2-D) unsteady shock reflection over a single wedge is studied theoretically and numerically, and the emphasis is placed on the trajectory of the triple point (TP). Skews' relation and the three-shock theory are, respectively, used for determining the trajectory angles of the corner-generated disturbance and the TP, and, subsequently, a model capable of predicting the TP trajectory is established for 2-D unsteady shock reflections over a single wedge. Then, a systematically numerical study is carried out on the 2-D unsteady shock reflection over a single wedge, including five types of shock reflection with the wedge angle increased and five types of shock reflection with the wedge angle decreased. It is found that the Mach stem is always slightly concavely (convexly) curved for reflections with the wedge angle increased (decreased), which should be caused by corner-generated compression (rarefaction) waves propagating along the Mach stem. The new model reasonably predicts the TP trajectory in all the 2-D unsteady shock reflections, and its performance is related not only to the variation trend of the wedge angle (increase or decrease), but also to the type of shock and the initial wedge angle. Specifically, for the shock reflection with the wedge angle increased (decreased), the model generally provides a slightly better (worse) prediction if the TP trajectory angle calculated by the three-shock theory is compulsively modified. The shock-shock/expansion polar analysis presented can partially explain the model performance for predicting the TP trajectory.

Key words: shock waves

1. Introduction

When a shock wave obliquely encounters a wedge, shock reflection occurs (Ben-Dor 2007). There are two types of shock reflection, including regular reflection (RR) and Mach

† Email address for correspondence: sanjing@ustc.edu.cn

© The Author(s), 2022. Published by Cambridge University Press

https://doi.org/10.1017/jfm.2022.688 Published online by Cambridge University Press

reflection (MR) (Mach 1878). The RR configuration consists of an incident shock and a reflected shock, while the MR consists of four discontinuities, including an incident shock, a reflected shock, a Mach stem and a slip line. In the MR, the intersection point of the four discontinuities is called the triple point (TP), which is crucial to determine the interactions among those discontinuities. Up to now, steady and pseudo-steady shock reflections have achieved a clear theoretical description, while there are still many unsolved problems in the unsteady shock reflection (Ben-Dor 2007). Generally speaking, the MR $\rightarrow$ RR transition and RR $\rightarrow$ MR transition are the two fundamental problems of unsteady shock reflection, and the MR $\rightarrow$ RR transition is closely related to the TP trajectory. Therefore, the TP trajectory and these two transitions have gained extensive attention for decades. The RR $\rightarrow$ MR transition in a wide variety of unsteady shock reflections over a convex or a straight wedge has been investigated (Wang & Zhai 2020), and it was found that the pseudo-steady criterion is capable of predicting the transition because the corner-generated disturbance cannot overtake the reflection point before the pseudo-steady criterion is reached. Prediction of the MR $\rightarrow$ RR transition and the TP trajectory in the unsteady shock reflection, however, still remains a challenge in theory. Investigation of the TP trajectory in unsteady shock refection remains especially desirable because the TP trajectory not only reflects the flow unsteadiness, but also determines whether and where the MR $\rightarrow$ RR transition would occur. In addition, the flow and transient dynamic load induced by cylindrical/spherical blast wave reflection (Dewey, McMillin & Classen 1977; Dewey & McMillin 1981; Liang, Hsu & Wang 2001; Liang, Wang & Chen 2002) and the flow pressure histories and features in shock focusing (Sturtevant & Kulkarny 1976; Skews & Kleine 2007) are highly related to the unsteady shock reflection process, and, therefore, closely related to the TP trajectory. As a result, the MR $\rightarrow$ RR transition and the TP trajectory have received increasing attention in the unsteady shock reflection study.

The flow behind the Mach stem is subsonic with respect to the TP, which means that the disturbance behind the Mach stem would affect the flow in the TP vicinity. To describe the TP trajectory in the MR, one should properly treat this disturbance under different flow conditions, i.e. pseudo-steady flow or unsteady flow. In the pseudo-steady MR, because the boundary condition is stationary, the wave configuration is stable. Provided that the Mach stem is straight and perpendicular to the wedge (Ben-Dor 2007), the TP movement can be approximately described by the three-shock theory proposed by von Neumann (1943*a*,*b*) and the ray-shock theory which was first proposed by Whitham (1957) and later modified by Milton (1975) and Itoh, Okazaki & Itaya (1981). We note that a curved Mach stem usually forms in reality, and the theoretical prediction accuracy is often limited. For the unsteady MR, the TP propagation would be affected by disturbances generated at the position where boundary conditions change, causing an unsteady movement of the TP. It will take some time for the disturbances, which carry the information of the variation of boundary conditions, to overtake the TP and affect its movement. In other words, there is a hysteresis in the response of the TP propagation to the variation of boundary conditions, which makes the theoretical prediction of the TP trajectory in unsteady flow very difficult.

The shock reflecting over a wedge is a typical configuration for the shock reflection study. In our previous work (Wang *et al.* 2017), a specially curved wedge for eliminating wedge angle effect was designed for convergent cylindrical shock reflection. In other words, when a convergent cylindrical shock reflects over the specific curved wedge, the wedge angle is constant. For convergent cylindrical shock reflection, the shape of the specific curved wedge must be convex. If the curvature of the convex wedge is larger than that of the specific convex wedge, the wedge angle is reduced when a convergent

https://doi.org/10.1017/jfm.2022.688 Published online by Cambridge University Press

cylindrical shock reflects from the wedge. On the contrary, if the curvature of the convex wedge is smaller than that of the specific convex wedge, the wedge angle is increased when a convergent cylindrical shock reflects from the wedge. Besides, if the wedge is planar or concavely curved, the wedge angle is also increased when a convergent cylindrical shock reflects from the wedge. Similarly, for a divergent cylindrical shock reflection, to guarantee a constant wedge angle, the curved wedge must be concave. If the curvature of the concave wedge is larger than that of the specific concave wedge, the wedge angle is increased when a divergent cylindrical shock reflects from the wedge. On the contrary, if the curvature of the concave wedge is smaller than that of the specific concave wedge, the wedge angle is reduced when a divergent cylindrical shock reflects from the wedge. Besides, if the wedge is planar or convexly curved, the wedge angle is also reduced when a divergent cylindrical shock reflects from the wedge. As a result, there are five types of unsteady shock reflection with the wedge angle increased, including a planar shock reflection over a concave wedge, a convergent cylindrical shock reflection over a straight/concave/convex wedge and a divergent cylindrical shock reflection over a concave wedge; and five types of unsteady shock reflection with the wedge angle reduced, including a planar shock reflection over a convex wedge, a divergent cylindrical shock reflection over a straight/convex/concave wedge and a convergent cylindrical shock over a convex wedge. The differing types of curved shock reflections have been classified and schematically illustrated in our previous work (Wang & Zhai 2020), where readers can find more details.

The reflections of a planar shock over a concave/convex wedge have been extensively investigated. The study of the planar shock reflecting over a concave wedge is mainly related to the formation of the von Neumann reflection or MR (Skews & Kleine 2007, 2009; Gruber & Skews 2013; Cohen & Skews 2020; MacLucas, Skews & Kleine 2020) and the TP trajectory prediction. The first attempt to predict the TP trajectory was carried out by Itoh *et al.* (1981). By using a modified Chester–Chisnell–Whitham relation (Chester 1954; Chisnell 1957; Whitham 1957), the TP trajectory and the MR $\rightarrow$ RR transition angle in cases of weak and moderately strong shock waves were obtained. Based on the length-scale concept proposed by Hornung, Oertel & Sandeman (1979), the MR $\rightarrow$ RR transition has been studied (Ben-Dor & Takayama 1985). Assuming that the corner-generated signals move along two different specific paths, two formulas for predicting the MR $\rightarrow$ RR transition angle were proposed. It should be noted that when a shock wave reflects over a curved wedge, disturbances are generated continuously, and, consequently, the TP will be influenced by these disturbances continuously. However, this process was ignored or not fully considered in the models of Itoh *et al.* (1981) and Ben-Dor & Takayama (1985). To better understand the reflection process, the shock reflection over a curved wedge can be divided into many mini-double-wedge shock reflections (Ben-Dor, Dewey & Takayama 1987; Li & Ben-Dor 1999; Xie, Han & Takayama 2005; Krassovskaya & Berezkina 2017; Wang & Zhai 2020; Yuan *et al.* 2020). Based on this concept, the unsteady reflection of a planar shock over various concave ramps has been numerically studied (Krassovskaya & Berezkina 2017), and the wave configurations were found to be determined by complex sub-processes and cannot be described by the three-shock theory. Yuan *et al.* (2020) found that the TP trajectory angle predicted by the three-shock theory is usually larger than that obtained from the computation in the pseudo-steady flow. Then they modified the prediction of the three-shock theory by applying the two-shock theory, and obtained a relatively accurate prediction of the TP trajectory. However, the model proposed by Yuan *et al.* (2020) is only applicable to the planar shock reflection with the wedge angle increased because the trajectory angle of the corner-generated disturbance is still predicted by the three-shock theory.

https://doi.org/10.1017/jfm.2022.688 Published online by Cambridge University Press

Recently, Koronio *et al.* (2020) studied the reflection of a planar shock over a concave wedge with different initial conditions (including different ambient gases, different wedge curvatures and different shock strengths) numerically and theoretically. Based on the shock dynamics concept (Han & Yin 1993) and gas dynamics point of view, the reflection process and the mechanism of the similarity of it in different initial conditions were interpreted in detail. For a planar shock reflecting over a convex wedge, most studies focused on the RR $\rightarrow$ MR transition (Skews & Kleine 2009, 2010; Hakkaki-Fard & Timofeev 2012; Geva, Ram & Sadot 2018; Wang & Zhai 2020), whereas the studies on the TP trajectory after the RR $\rightarrow$ MR transition occurs were rare (Itoh *et al.* 1981; Kleine *et al.* 2014). Itoh *et al.* (1981) considered the theoretical position when the RR $\rightarrow$ MR transition occurs as the starting point of the TP trajectory, and studied the TP trajectory by the characteristics method (Bryson & Gross 1961). The viscosity effect on the TP trajectory has been studied by Kleine *et al.* (2014). They found that the viscosity hinders the emergence of the RR $\rightarrow$ MR transition, but has limited effect on the flow once the RR $\rightarrow$ MR transition occurs.

For the remaining types of curved shock reflections, however, there are only a few studies. Zhang *et al.* (2016) and Gray & Skews (2017) studied a convergent shock reflection over a straight wedge, and found that the pseudo-steady criterion fails to predict the MR $\rightarrow$ RR transition which is highly related to the TP trajectory because of the flow unsteadiness. Assuming that the analysis for the pseudo-steady flow can be applied to the reflection of a blast wave (can be regarded as a divergent shock to a certain extent) over a planar surface, Hu & Glass (1986) proposed a simple geometrical model for predicting the TP trajectory. By extending the works of Itoh *et al.* (1981) and Ben-Dor & Takayama (1985) to the convergent circumstance, Ndebele & Skews (2018) achieved the predictions of the Mach stem length variation and the MR $\rightarrow$ RR transition angle in the reflection of a convergent cylindrical shock wave over a cylindrical concave wedge. However, it is still a challenge to establish a general theory to describe the unsteady shock reflection, especially in the planar shock reflection with the wedge angle decreased and in the curved shock reflections. This motivates the present study.

In this study we shall treat the disturbance propagation process by using Skews' relation, which will be defined later. Then, by assuming the flow in the TP vicinity immediately adapts to the new boundary conditions at the position where the disturbance is generated, the TP trajectory angle is obtained by applying the three-shock theory. In this way, a model for predicting the TP trajectory will be established for all known types of two-dimensional (2-D) unsteady reflections over a single wedge. Then, extensive inviscid numerical simulations are performed for the ten types of 2-D unsteady shock reflections over a single wedge, and the emphasis will be placed on evaluating the model. Note that a relatively straight Mach stem is necessary to assure the accuracy of the three-shock theory. To provide a relatively straight Mach stem, the incident shock with a Mach number of 2.0 and a wedge angle greater than 20° are imposed in this work.

2. Model for TP trajectory prediction

In the model proposed by Yuan *et al.* (2020), the three-shock theory was applied to calculate the trajectory angle of the corner-generated disturbance propagating along the Mach stem. However, the three-shock theory is not always solvable especially when a weak shock wave reflects over a wedge with a small angle. For example, when a shock reflects over a wedge with a small angle, von Neumann reflection (vNR), Guderley reflection (GR) and Vasilev reflection (VR) may occur (Guderley 1962; Colella & Henderson 1990;

https://doi.org/10.1017/jfm.2022.688 Published online by Cambridge University Press

Vasil'ev 1999; Vasil'ev & Kraiko 1999; Tesdall & Hunter 2002; Skews & Ashworth 2005; Tesdall, Sanders & Keyfitz 2008; Vasil'ev, Elperin & Ben-Dor 2008; Skews, Li & Paton 2009; Viero, Susin & Defina 2013). These wave configurations resemble a MR configuration. For vNR, the three-shock theory can provide a non-standard physical solution. However, for GR and VR, the three-shock theory could not provide a physical solution. This phenomenon is known as the von Neumann paradox (Vasil'ev *et al.* 2008). Therefore, their model is only applicable when the shock wave is strong. Besides, since the three-shock theory is only applicable when the wedge angle variation is positive, their model can only predict the TP trajectory in the shock reflection with the wedge angle increased. In the 2-D unsteady shock reflection over a single wedge, if the wedge angle varies slowly, the corner-generated disturbances are so weak that they can be treated as sound waves. Skews (1967) once proposed a relation using the theory of sound to calculate the trajectory angle of the first sound wave produced from the corner, and this relation is called Skews' relation in this work. According to Skews' relation, for the shock reflection with the wedge angle either increased or decreased, although the type of corner-generated disturbance is different, the disturbance propagation process is the same. The application of Skews' relation to predict the trajectory angle of the weak disturbance (χ^D) is irrelevant to the disturbance type. As a result, Skews' relation can be applied to a shock reflection with the wedge angle increased or decreased. This provides a possibility to establish a model for the TP trajectory prediction. The basic principle of the model is to combine Skews' relation and the three-shock theory to predict the trajectory angles of the corner-generated disturbance propagating along the Mach stem and the TP propagating along the incident shock, respectively. Further, it is assumed that when the TP is overtaken by corner-generated disturbance, the flow in the TP vicinity immediately adapts to the new boundary conditions at the position where the disturbance is generated. In this section we first establish the model for the planar shock reflection and then for the convergent/divergent cylindrical circumstance.

The propagation process of the disturbance when a planar shock reflects over a convex wedge is sketched in figure 1, in which the reflected shock waves and slip lines are ignored for simplicity. The smooth convex wedge can be viewed as an infinite set of straight sub-wedges, and the first sub-wedge is denoted by AB. Provided that the wedge angle of the first sub-wedge ω_1 is smaller than ω_d (the RR $\leftrightarrow$ MR transition wedge angle predicted by the detachment criterion), a MR (a direct-Mach reflection in fact) forms with the first TP (T_1) and the first Mach stem m_1 when the incident shock collides with point A. Note that the shock movement over the first sub-wedge AB is a quasi-pseudo-steady flow, and a small Mach stem will form immediately at point A. However, the height of the Mach stem at point A is infinitesimal, and is considered as zero in the following formulation. This treatment has widely been adopted in previous works (Ben-Dor 2007; Dewey & McMillin 1985; Ben-Dor *et al.* 1987, 1988; Li & Ben-Dor 1999; Xie *et al.* 2005). During m_1 moving along the sub-wedge AB, the velocity of T_1 propagating along the incident shock is constant and the trajectory angle of T_1 (χ_1^T) can be predicted by the three-shock theory. As long as χ_1^T is known, the Mach number of m_1 (M_1^m) can be calculated by

$$M_1^m = \frac{M_0 \cos \chi_1^T}{\cos(\omega_1 + \chi_1^T)}, \tag{2.1}$$

where M_0 is the Mach number of the incident shock. When the Mach stem m_1 meets the next sub-wedge BC, the boundary condition changes and the m_1 is not perpendicular to BC. Because the wedge is convexly curved and the variation of the wedge angle relative

https://doi.org/10.1017/jfm.2022.688 Published online by Cambridge University Press

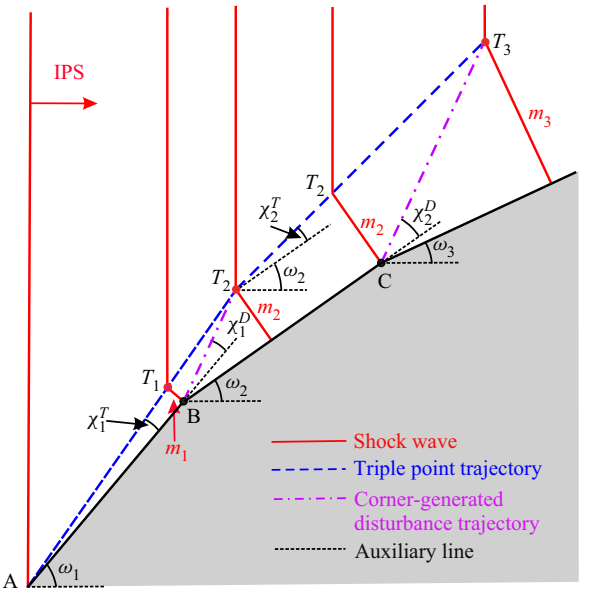


Figure 1. Disturbance propagation process in the reflection of a planar shock over a convex wedge, in which reflected shock waves and slip lines are ignored for simplicity. Here IPS stands for incident planar shock; T_1, T_2 and T_3 are TPs; m_1, m_2 and m_3 are Mach stems; ω_1, ω_2 and ω_3 are wedge angles of corners; χ_1^T and χ_2^T are trajectory angles of the first and second TPs T_1 and T_2, respectively; χ_1^D and χ_2^D are trajectory angles of the first and second corner-generated disturbances from corners B and C, respectively.

to the m_1 is very small (far less than 1°), a weak disturbance (rarefaction wave) is formed from point B and propagates along the m_1 (for a concave wedge, a compression wave rather than a shock wave will be formed). The weak disturbance can be taken as a sound wave, and Skews' relation can be used to calculate its trajectory. In the present work the Mach stem m_1 serves as the 'incident shock', and the trajectory angle of the weak disturbance χ_1^D can be calculated as long as M_1^m is known by Skews' relation (Skews 1967), which is expressed as

$$\tan \chi_1^D = \left\{ \frac{[(M_1^m)^2 - 1][(\gamma - 1)(M_1^m)^2 + 2]}{(\gamma + 1)(M_1^m)^4} \right\}^{1/2}, \tag{2.2}$$

where γ is the specific heat ratio. We here clarify that (2.2) is an engineering estimate and has limitations in the applicability. Before the corner-generated disturbance catches up with the T_1, the trajectory angle of T_1 remains constant. As a result, there is a hysteresis in the response of the TP propagation to the variation of boundary conditions. Once the disturbance meets the T_1, both the T_1 and the m_1 disappear, and a new TP (T_2) moving along the incident shock and a new Mach stem m_2 form. The coordinates of T_2 when it forms (x_2^T, y_2^T) can be solved by the following equations:

$$y_2^T = y_1 + (x_2^T - x_1)\tan(\omega_1 + \chi_1^T), \tag{2.3}$$

$$y_2^T = y_2 + (x_2^T - x_2)\tan(\omega_1 + \chi_1^D). \tag{2.4}$$

Here (x_1, y_1) and (x_2, y_2) are coordinates of points A and B in the Cartesian coordinate system, respectively.

https://doi.org/10.1017/jfm.2022.688 Published online by Cambridge University Press

When the TP is overtaken by the corner-generated disturbance, provided that the flow in the TP vicinity immediately adapts to the new boundary conditions at the position where the disturbance is generated (this assumption will be discussed in Appendix A), the trajectory angle of T_2 moving along the incident shock (χ_2^T) can be calculated by substituting ω_2 (the wedge angle of the second sub-wedge BC) and M_0 into the three-shock theory. Similarly, the Mach number of m_2 and the trajectory angle of the disturbance generated from point C (χ_2^D) can be obtained. Further, the coordinates of the third TP (T_3) when it forms can be solved by trajectory equations of the T_2 and the disturbance formed from point C. Similar relations can be extended and the coordinates of the ith TP when it forms (x_i^T, y_i^T) are solved by

$$y_i^T = y_{i-1}^T + (x_i^T - x_{i-1}^T)\tan(\omega_{i-1} + \chi_{i-1}^T), \tag{2.5}$$

$$y_i^T = y_i + (x_i^T - x_i)\tan(\omega_{i-1} + \chi_{i-1}^D), \tag{2.6}$$

where (x_{i-1}^T, y_{i-1}^T) and $(x_i,\ y_i)$ are coordinates of the $(i-1)$th TP when it forms and the ith corner, respectively; ω_{i-1} is the wedge angle of the $(i-1)$th sub-wedge, χ_{i-1}^T and χ_{i-1}^D are trajectory angles of the $(i-1)$th TP propagating along the incident shock and the disturbance generated at the ith corner propagating along the $(i-1)$th Mach stem, respectively. Extending the model from the planar shock reflection to the convergent/divergent shock reflection is rather straightforward. As sketched in figure 2, the convergent/divergent cylindrical shock over a concave wedge with the wedge angle increased is considered and a polar coordinate system centred on the convergent/divergent centre (point O) is established. Provided that ω_1 is smaller than ω_d, a MR with T_1 and m_1 forms when the incident shock coincides with point A. Here χ_1^T can be calculated by the three-shock theory, and M_1^m and χ_1^D can also be calculated if χ_1^T is known. Over the first sub-wedge AB with the constant wedge angle, the intensity of the disturbance propagating along the incident shock is almost unvaried. In our previous work (Wang *et al.* 2017), it was found that the behaviour of the disturbance propagating along the incident shock in the curved shock circumstance is the same as that in the planar shock circumstance in an infinitely short reflection process. According to this principle, the trajectory equation of the T_1 can be obtained as

$$r = r_1\,\mathrm{e}^{(\theta-\theta_1)\cot(\omega_1+\chi_1^T)}, \tag{2.7}$$

where (r_1, θ_1) are coordinates of point A. The derivation of this relation for cylindrically convergent shock reflection can be found in our previous work (Wang *et al.* 2017), and its extension to cylindrically divergent reflection can be found in Appendix B. The trajectory of the corner-generated disturbance propagating along the Mach stem in the convergent/divergent circumstance can be approximately taken as a straight line as long as the curvature of the Mach stem is limited. The trajectory equation of the disturbance generated at point B is

$$y = y_2 + (x - x_2)\tan(\omega_1 + \theta_1 + \chi_1^D). \tag{2.8}$$

The coordinates of the second TP when it forms can be solved by (2.7) and (2.8). Similarity, χ_2^T and χ_2^D can be calculated by the three-shock theory and Skews' relation, respectively. Similar relations can be extended to obtain the coordinates of the ith TP when

https://doi.org/10.1017/jfm.2022.688 Published online by Cambridge University Press

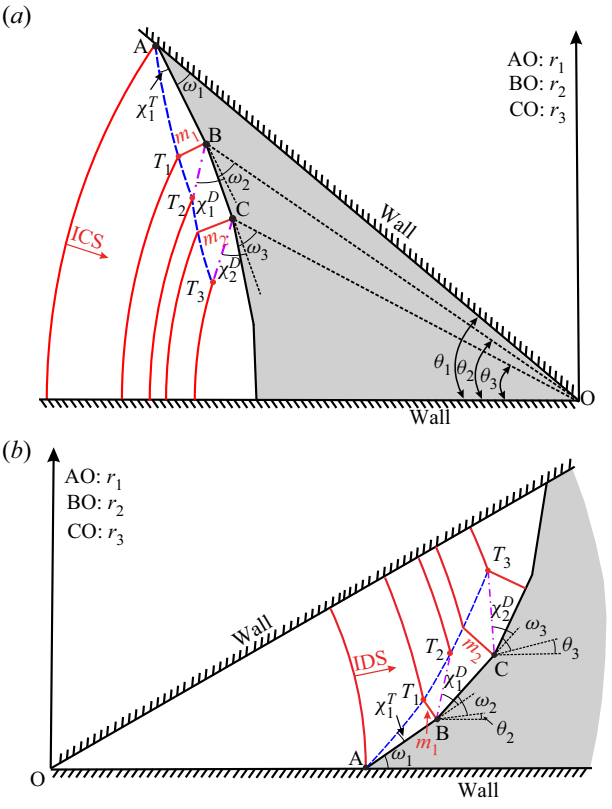


Figure 2. Disturbance propagation process of a convergent (*a*) and a divergent (*b*) shock reflection over a concave wedge with the wedge angle increased. Here ICS stands for incident convergent shock and IDS stands for incident divergent shock; θ_1, θ_2 and θ_3 are polar angles of the first three corners. The other symbols are the same as those in figure 1.

it forms,

$$r = r_{i-1}^T \, \mathrm{e}^{(\theta-\theta_{i-1}^T)\cot(\omega_{i-1}+\chi_{i-1}^T)}, \tag{2.9}$$

$$y = y_i + (x - x_i)\tan(\omega_{i-1} + \theta_{i-1} + \chi_{i-1}^D), \tag{2.10}$$

where $(r_{i-1}^T, \theta_{i-1}^T)$ are coordinates of the $(i-1)$th TP when it forms.

3. Numerical method and wedge design

To study all known types of 2-D unsteady shock reflections over a single wedge and also validate the model proposed above, extensive inviscid numerical simulations are performed. In this work the numerical solver VAS2D (2-D vectorized adaptive solver) (Sun & Takayama 1999), which has been well validated in shock-body interactions (Zhang *et al.* 2016; Wang *et al.* 2017; Wang & Zhai 2020) and shock-interface interactions (Zhai *et al.* 2011, 2014, 2018; Zhai, Ou & Ding 2019*a*), is employed. In the numerical algorithm, the 2-D compressible Euler equations are adopted as the governing equations, which can be written in the vectorial form

$$\frac{\partial \boldsymbol{U}}{\partial t} + \frac{\partial \boldsymbol{F}}{\partial x} + \frac{\partial \boldsymbol{G}}{\partial y} = 0, \tag{3.1}$$

https://doi.org/10.1017/jfm.2022.688 Published online by Cambridge University Press

where $\boldsymbol{U}$, $\boldsymbol{F}$ and $\boldsymbol{G}$ represent the conserved variables, the convective fluxes in the x- and y-directions, respectively, i.e.

$$\boldsymbol{U} = \begin{pmatrix} \rho \\ \rho u \\ \rho v \\ \rho E \end{pmatrix}; \quad \boldsymbol{F} = \begin{pmatrix} \rho u \\ \rho u^2 + p \\ \rho uv \\ (\rho E + p)u \end{pmatrix}; \quad \boldsymbol{G} = \begin{pmatrix} \rho v \\ \rho uv \\ \rho v^2 + p \\ (\rho E + p)v \end{pmatrix}, \tag{3.2a–c}$$

where p, ρ, E, u and v, respectively, represent the pressure, density, total energy per unit mass and velocity components in the x- and y-directions.

The finite volume method is used to discretize the conservation laws by applying them directly to each non-overlapping control volume. The MUSCL–Hancock approach is adopted to reach a second-order precision in both temporal and spatial scales. To refine the local complex areas and capture the wave configurations effectively, an unstructured adaptive mesh is used. The current criterion for adaptation is based on the truncation error of the Taylor series expansion of density. The truncation error indicator ε_T is given by the ratio of the second-order derivative term to the first-order one in Taylor expansion. If $\varepsilon_T > \varepsilon_r$, the cell needs to be refined, and if $\varepsilon_T < \varepsilon_c$, the cell needs to be coarsened, where ε_r and ε_c are threshold values for refinement and coarsening. In the computations, the ambient air is assumed to be a perfect gas, and the initial temperature and pressure are 293 K and 101 325 Pa, respectively. The initial mesh size of 0.3 mm and the finest mesh size of 18.8 μm in the positions where greater density gradient exists are applied. Grid convergence validation has been conducted in our previous works (Wang & Zhai 2020; Wang, Zhai & Luo 2021), and a grid with a similar size to the previous work is adopted in this work.

In numerical simulations the Mach number of the convergent or divergent shock varies very slowly, which results in a very small variation of χ^T predicted by the three-shock theory (Ben-Dor *et al.* 1987; Wang *et al.* 2017). Therefore, the Mach number of the incident shock can be considered as a constant in theoretical calculations. Note that the three-shock theory is relatively accurate in predicting χ^T when the Mach stem is straight. However, when the incident shock is weak ($M_0 < 1.5$ for example), the Mach stem tends to be concavely curved (Dewey & McMillin 1985; Olim & Dewey 1992; Henderson *et al.* 2003), probably because the disturbances generated by the flow-deflection process overtake the TP and affect the Mach stem shape since the flow behind the reflected shock wave with respect to the TP is subsonic. When the incident shock is strong ($M_0 > 3.0$ for example), the Mach stem tends to be convexly curved (Hornung 1986; Henderson *et al.* 2003; Shi *et al.* 2019), because a wall jet is generated and causes the convex bending of the Mach stem. To provide a relatively straight Mach stem, the incident shock with a Mach number of 2.0 and a wedge angle greater than 20° are imposed in this work. This choice also avoids the problem that the three-shock theory is not always solvable for the MR over a wedge with a small angle (Xie *et al.* 2005), especially when the shock wave is weak. Furthermore, to ensure the prediction accuracy and the physical correctness of the application of Skews' relation for finding χ^D, the absolute value of wedge angle variation in each iteration should be far less than 1°. In this work, the number of iterations in calculation is fixed at 2500 and the wedge angle variation in each iteration is $(\omega_t - \omega_0)/2500$, where ω_0 and ω_t are wedge angles at the leading and trailing edges of the wedge, respectively.

The unsteady shock reflection over a single wedge can be roughly divided into two classes, wedge angle increased and wedge angle decreased. As discussed before, there are five types of shock reflection with wedge angle increased, including a planar shock reflection over a concave wedge, a convergent cylindrical shock reflection over a

https://doi.org/10.1017/jfm.2022.688 Published online by Cambridge University Press

Shock type	Wedge type	Wedge angle variation	Requirement of $\mathrm{d}\omega$
Convergent	Straight	Increase	$\mathrm{d}\omega = -\mathrm{d}\theta$
Convergent	Concave	Increase	$\mathrm{d}\omega > -\mathrm{d}\theta$
Convergent	Convex	Increase	$0^\circ < \mathrm{d}\omega < -\mathrm{d}\theta$
Convergent	Convex	Decrease	$\mathrm{d}\omega < 0^\circ$
Divergent	Straight	Decrease	$-\mathrm{d}\omega = \mathrm{d}\theta$
Divergent	Convex	Decrease	$-\mathrm{d}\omega > \mathrm{d}\theta$
Divergent	Concave	Decrease	$0^\circ < -\mathrm{d}\omega < \mathrm{d}\theta$
Divergent	Concave	Increase	$-\mathrm{d}\omega < 0^\circ$

Table 1. Summary of the wedge shapes for convergent/divergent cylindrical shock reflections with the wedge angle increased or decreased and the requirement of $\mathrm{d}\omega$ at each position on the wedge.

straight/concave/convex wedge and a divergent cylindrical shock reflection over a concave wedge; and five types of shock reflection with wedge angle reduced, including a planar shock reflection over a convex wedge, a divergent cylindrical shock reflection over a straight/convex/concave wedge and a convergent cylindrical shock over a convex wedge. For investigating curved shock reflection over a curved wedge, the wedge should be carefully designed according to the type of shock (convergent or divergent) and variation trend of the wedge angle (increase or decrease). According to our previous work (Zhang *et al.* 2016; Wang *et al.* 2017), during a convergent cylindrical shock moving along a straight wedge, the geometric effect of the convergent shock causes an increase of the wedge angle, and the variation rate of ω equals the negative of the variation rate of θ ($\mathrm{d}\omega = -\mathrm{d}\theta$). Therefore, to design a concave (convex) wedge for a convergent shock reflection in the polar coordinate system, the variation rate of ω must be larger (smaller) than the negative of the variation rate of θ, i.e. $\mathrm{d}\omega > -\mathrm{d}\theta$ ($\mathrm{d}\omega < -\mathrm{d}\theta$) at each position on the wedge (Wang & Zhai 2020). Similarly, the geometric effect of the divergent shock causes a reduction of the wedge angle, and the negative of the variation rate of ω equals the variation rate of θ ($-\mathrm{d}\omega = \mathrm{d}\theta$). As a result, to design a concave (convex) wedge for a divergent shock reflection in the polar coordinate system, the negative of the variation rate of ω must be smaller (larger) than the variation rate of θ, i.e. $-\mathrm{d}\omega < \mathrm{d}\theta$ ($-\mathrm{d}\omega > \mathrm{d}\theta$) at each position on the wedge. Table 1 summarizes the wedge shapes for convergent/divergent shock reflections with the wedge angle increased or decreased and the requirement of $\mathrm{d}\omega$ at each position on the wedge.

The computational domains are sketched in figure 3 for four typical cases: a planar shock reflecting over a concave wedge, a planar shock over a convex wedge, a convergent shock over a straight wedge and a divergent shock over a straight wedge. Note that the scales in the figure do not reflect the real ones. For all cases, the inlet condition is applied to the left boundary (blue solid lines), while solid-wall conditions are applied to the other boundaries and the wedge (black solid lines). The initial post-shock flow is regarded as uniform, and the density, pressure and post-shock velocity are calculated from Rankine–Hugoniot relations. Note that the post-shock flow of a cylindrical shock is actually non-uniform. For a convergent or divergent cylindrical shock, its intensity varies very slowly when it is far away from the convergent centre or divergent centre (Zhai *et al.* 2012; Li *et al.* 2020), and the post-shock flow can approximately be regarded as uniform. In this work, although the initial post-shock flow is uniform, the post-shock flow varies as the cylindrical shock starts to move. In our previous work (Zhai *et al.* 2019*b*; Zhou *et al.* 2020) we numerically investigated the interaction of a convergent cylindrical shock with unperturbed and perturbed interfaces, and a uniform state behind the initially convergent

https://doi.org/10.1017/jfm.2022.688 Published online by Cambridge University Press

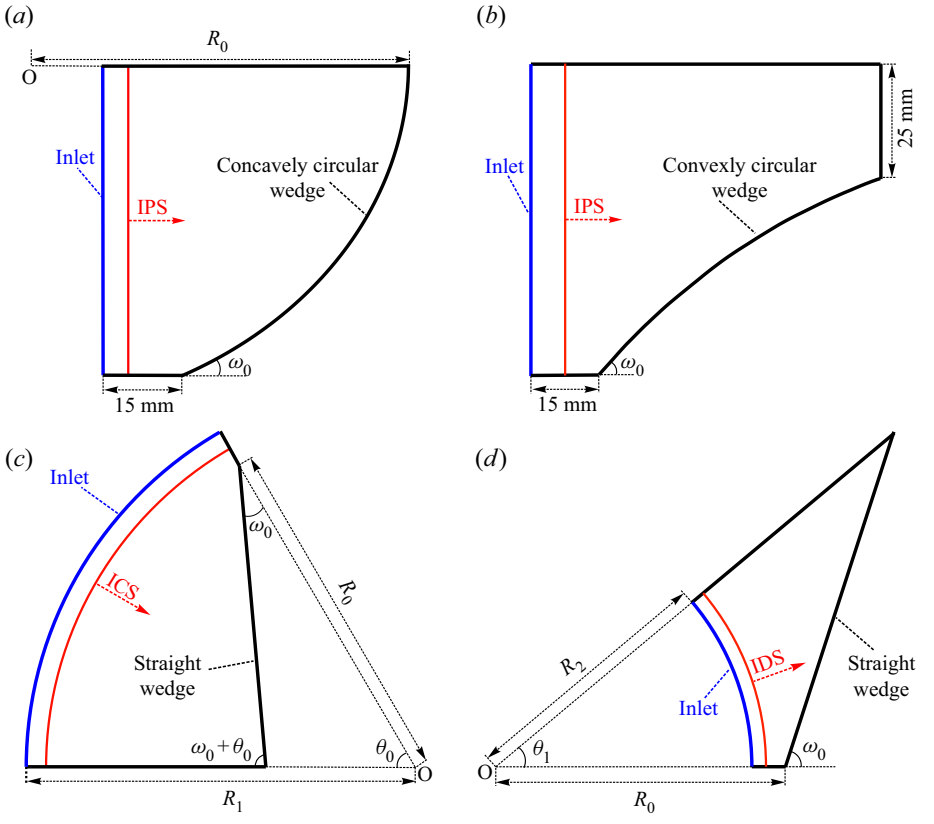


Figure 3. Computational domains of unsteady shock reflection over a single wedge. (*a*) A planar shock reflecting over a concave wedge, (*b*) a planar shock over a convex wedge, (*c*) a convergent shock over a straight wedge and (*d*) a divergent shock over a straight wedge.

shock was imposed. Through comparing the displacements of several shock waves and interface, and the interface amplitude growth between the numerical and experimental results, it was found that this approximation has a limited effect on the shock dynamics phenomena and post-shock flow features. As a result, a uniform state behind the initial shock is imposed in the present work for convenience.

For planar shock reflections, as sketched in figures 3(*a*) and 3(*b*), two different radii of a circular wedge (R_0) are considered: 100 and 150 mm, and the inlet is positioned at 15 mm away from the leading edge of the wedge. Specifically, for a planar shock reflection over a convex wedge, the wedge angle at the trailing edge of the wedge is 20°.

The computational domain of a convergent shock reflection over a straight wedge is sketched in figure 3(*c*). For the reflection of a convergent shock over a curved wedge, the straight wedge in figure 3(*c*) is simply replaced by a curved wedge with the specific shape, and the sketches of the corresponding computational domains are ignored. For cases with the straight wedge, the polar angle of the leading edge of the wedge (θ_0) is 60°. For cases with the concave wedge, $\theta_0 = 40°$ while the total variation of ω from the leading to trailing edges is chosen as 60°. Besides, ω changes linearly with θ : $\omega = \omega_0 + 1.5(\theta_0 - \theta)$ at each position on the wedge to ensure the concave shape of the wedge. For a convergent shock reflection over a convex wedge with the wedge angle increased, $\theta_0 = 80°$ while the total variation of ω from the leading to trailing edges of the wedge is set at 60°.

https://doi.org/10.1017/jfm.2022.688 Published online by Cambridge University Press

To ensure the convex shape of the wedge, ω changes linearly with θ : $\omega = \omega_0 + 0.75(\theta_0 - \theta)$ at each position on the wedge. For a convergent shock reflection over a convex wedge with the wedge angle reduced, to ensure the convex shape of the wedge, the wedge angle ω gradually reduces, and $\omega = \omega_0 - 1/3(\theta_0 - \theta)$ at each position on the wedge. Besides, θ_0 is chosen as 60° and the total variation of ω from the leading to trailing edges of the wedge is -20°. For all cases, two different R_0 (90 and 180 mm) are considered and the inlet is positioned at R_1 ($= R_0 + 10$ mm) away from the convergent centre. Note that for curved shock reflection, R_0 represents the radius of the leading edge of the wedge. To ensure that the Mach number of the incident convergent shock (ICS) is 2.0 when it meets the leading edge of the wedge, the initial incident shock Mach number is set at 1.9913 and its initial positions are set at 92.5 and 185 mm away from the convergent centre in cases with $R_0 = 90$ and 180 mm, respectively.

The computational domain of a divergent shock reflection over a straight wedge is sketched in figure 3(*d*). For the reflection of a divergent shock over a curved wedge, the straight wedge in figure 3(*d*) is simply replaced by a curved wedge with the specific shape, and the sketches of the corresponding computational domains are ignored. For cases with the straight wedge, $\theta_0 = 0^\circ$ and $\theta_1 = 20^\circ$ (θ_1 is the polar angle of the trailing edge of the wedge). The total variation of ω from the leading to trailing edges of the wedge is -20°. For cases with the convex wedge, $\theta_0 = 0^\circ$ and $\theta_1 = 15^\circ$. The total variation of ω from the leading to trailing edges of the wedge is -20°, and $\omega = \omega_0 - 4/3\theta$ at each position on the wedge to ensure the convex shape of the wedge. For a divergent shock reflection over a concave wedge with the wedge angle reduced, $\theta_0 = 0^\circ$ and $\theta_1 = 30^\circ$. The total variation of ω from the leading to trailing edges of the wedge is -20°, and $\omega = \omega_0 - 2/3\theta$ at each position on the wedge to ensure a decreased wedge angle of the concave wedge. For a divergent shock reflection over a concave wedge with the wedge angle increased, the total variation of ω from the leading to trailing edges of the wedge is 60°, and the increase of wedge angle ensures the concave shape of the wedge. Here θ_0 and θ_1 (the polar angle of the trailing edge of the wedge) are set at 0° and 40°, respectively. Besides, ω varies linearly with θ : $\omega = \omega_0 + 1.5\theta$ at each position on the wedge. For divergent shock reflections, two other different R_0 (100 and 150 mm) are considered and the inlet is positioned at R_2 ($= R_0 - 10$ mm) away from the divergent centre. To ensure that the Mach number of the incident divergent shock (IDS) is 2.0 when it meets the leading edge of the wedge, the initial Mach number of the IDS is set at 2.016 and its initial positions are set at 95 and 142.5 mm away from the divergent centre in cases with $R_0 = 100$ and 150 mm, respectively.

4. Results and discussion

We shall first study the unsteady shock reflection with the wedge angle increased and then one with the wedge angle decreased, and the emphasis is given to the TP trajectory. The TP trajectories from the theoretical prediction and the numerical result are compared. In comparison, we will also adopt the same modification proposed by Yuan *et al.* (2020) to see whether this modification is still effective or not in the unsteady case. As discussed before, in pseudo-steady shock reflection, the three-shock theory usually overestimates the TP trajectory angle. To obtain χ^T more accurately, the value predicted by the three-shock theory was modified by applying the two-shock theory (Yuan *et al.* 2020): $\chi^T_{mod}(\omega) = \chi^T_{ori}(\omega) - (\chi^T_{ori}(\omega_d)/\omega_d)\omega$. The subscripts 'ori' and 'mod' denote the original and modified predictions by the three-shock theory, respectively. This modification ensures

https://doi.org/10.1017/jfm.2022.688 Published online by Cambridge University Press

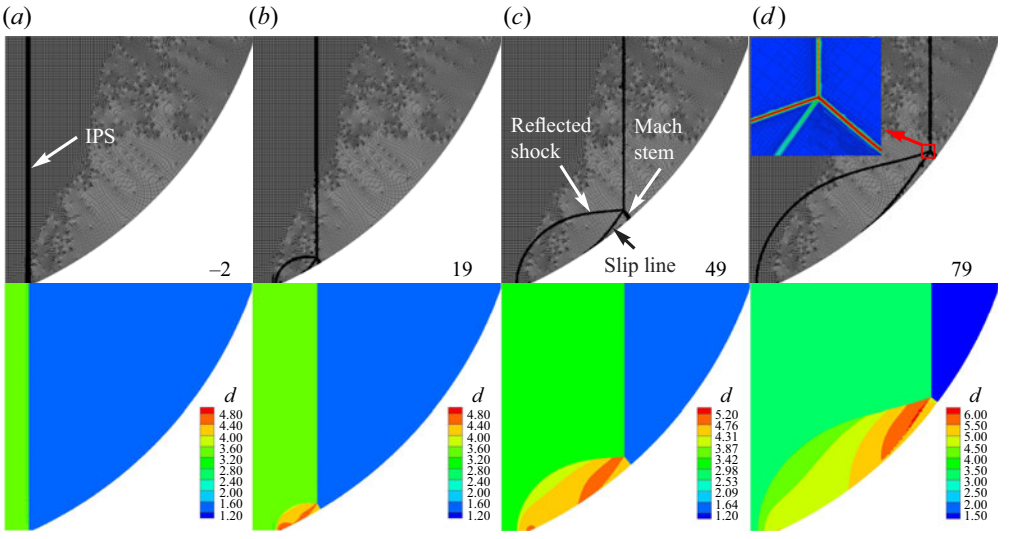


Figure 4. The computational meshes (top) and the corresponding density fields (bottom) of a planar shock reflection over a concave wedge with $\omega_0 = 25^\circ$ and $R_0 = 150$ mm at different moments. Numbers denote time in μs. The temporal origin is defined as the moment when the incident shock reaches the leading edge of the wedge, and similarly hereinafter.

that $\chi^T_{mod} = 0$ when $\omega = \omega_d$. When $M_0 = 2.0$, the detachment angle (ω_d) is 50.591° and $\chi^T_{ori}(\omega_d)$ is 1.046°, therefore, $\chi^T_{mod}(\omega) = \chi^T_{ori}(\omega) - (1.046/50.591)\omega$.

4.1. *Shock reflection with wedge angle increased*

We first consider the unsteady shock reflections with the wedge angle increased, and five different configurations, including a planar shock reflection over a concave wedge, a convergent shock reflection over a straight/concave/convex wedge and a divergent shock reflection over a concave wedge, are investigated. For all cases, three different initial wedge angles ω_0 (25°, 30° and 35°) are adopted.

Figure 4 shows the computational meshes (top) and the corresponding density fields (bottom) of a planar shock reflection over a concave wedge with $\omega_0 = 25^\circ$ and $R_0 = 150$ mm at different moments. Note that the numerical results are cropped to demonstrate the meshes and density fields more clearly. It can be found that the adaptation procedure refines the mesh in flow regions with a large density gradient (near the shock waves and slip line). The numerical schlieren images in figure 5 show the processes of five types of shock reflection with the wedge angle increased. For all cases, a MR is generated when the incident shock meets the leading edge of the wedge, and the Mach stem length first increases, then starts to decrease from the intermediate stages until the TP reaches the wedge. It is found that under the conditions considered, the Mach stem is always slightly concavely curved in shock reflection with the wedge angle increased, which should be caused by corner-generated compression waves propagating along the Mach stem. In planar and divergent shock reflections, the reflected shock in the vicinity of the TP is slightly convexly curved in the early stages, and gradually becomes slightly concavely curved in the late stages, while the slip line is always concavely curved. For the three types of convergent shock reflection, the reflected shock in the TP vicinity is convexly curved in all stages and its curvature decreases gradually, while the slip line is concavely

https://doi.org/10.1017/jfm.2022.688 Published online by Cambridge University Press

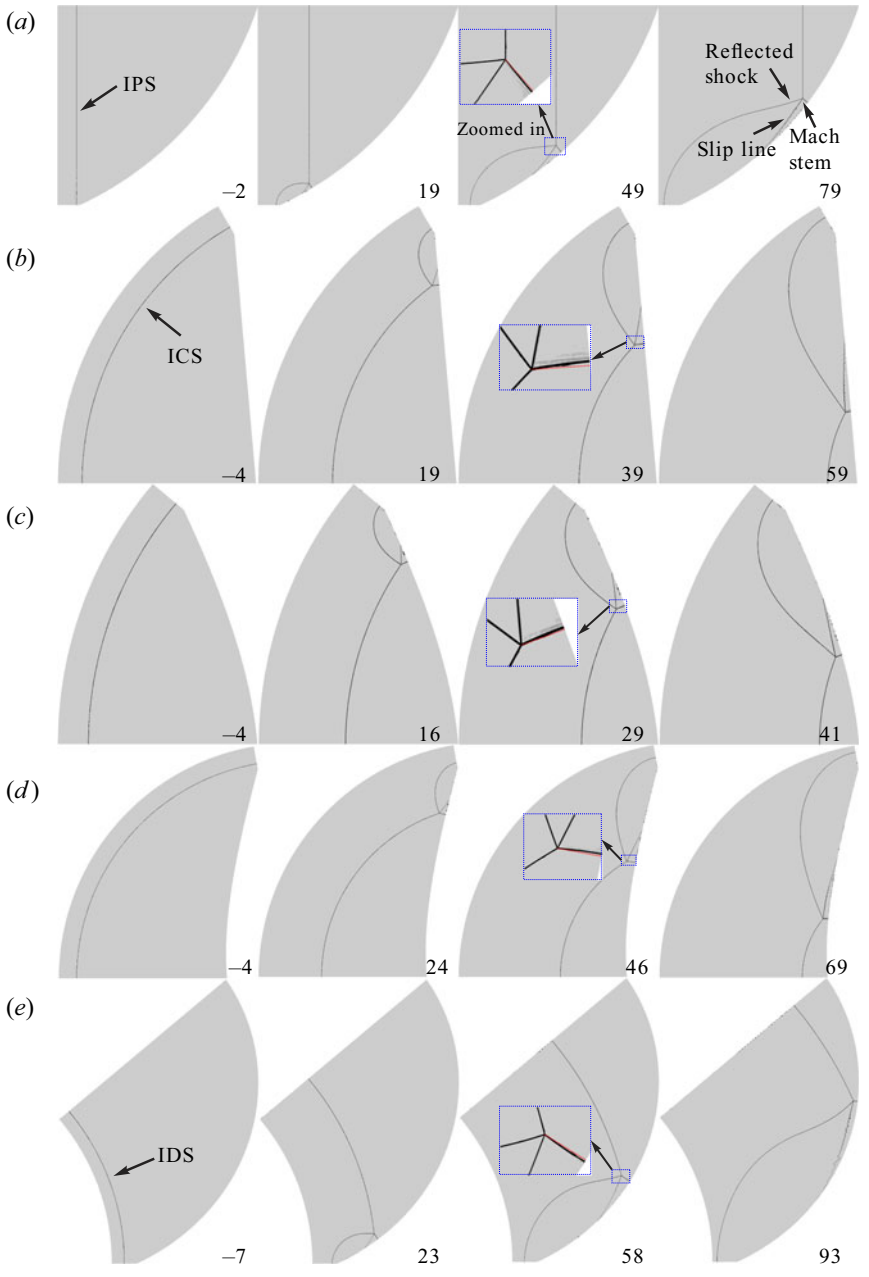


Figure 5. Shock reflection processes with the wedge angle increased. Planar shock over concave wedge with $\omega_0 = 25^\circ$ and $R_0 = 150$ mm (*a*). Convergent shock over straight wedge (*b*), concave wedge (*c*) and convex wedge (*d*) with $\omega_0 = 25^\circ$ and $R_0 = 90$ mm. Divergent shock over concave wedge with $\omega_0 = 25^\circ$ and $R_0 = 100$ mm (*e*).

curved in the early stages, and gradually becomes convexly curved in the late stages. From the comparison, we notice that the convergent shock contributes to making the reflected shock and the slip line convexly curved. The dimensionless TP trajectories from theoretical and numerical calculations are compared in figure 6. The identification method of the

https://doi.org/10.1017/jfm.2022.688 Published online by Cambridge University Press

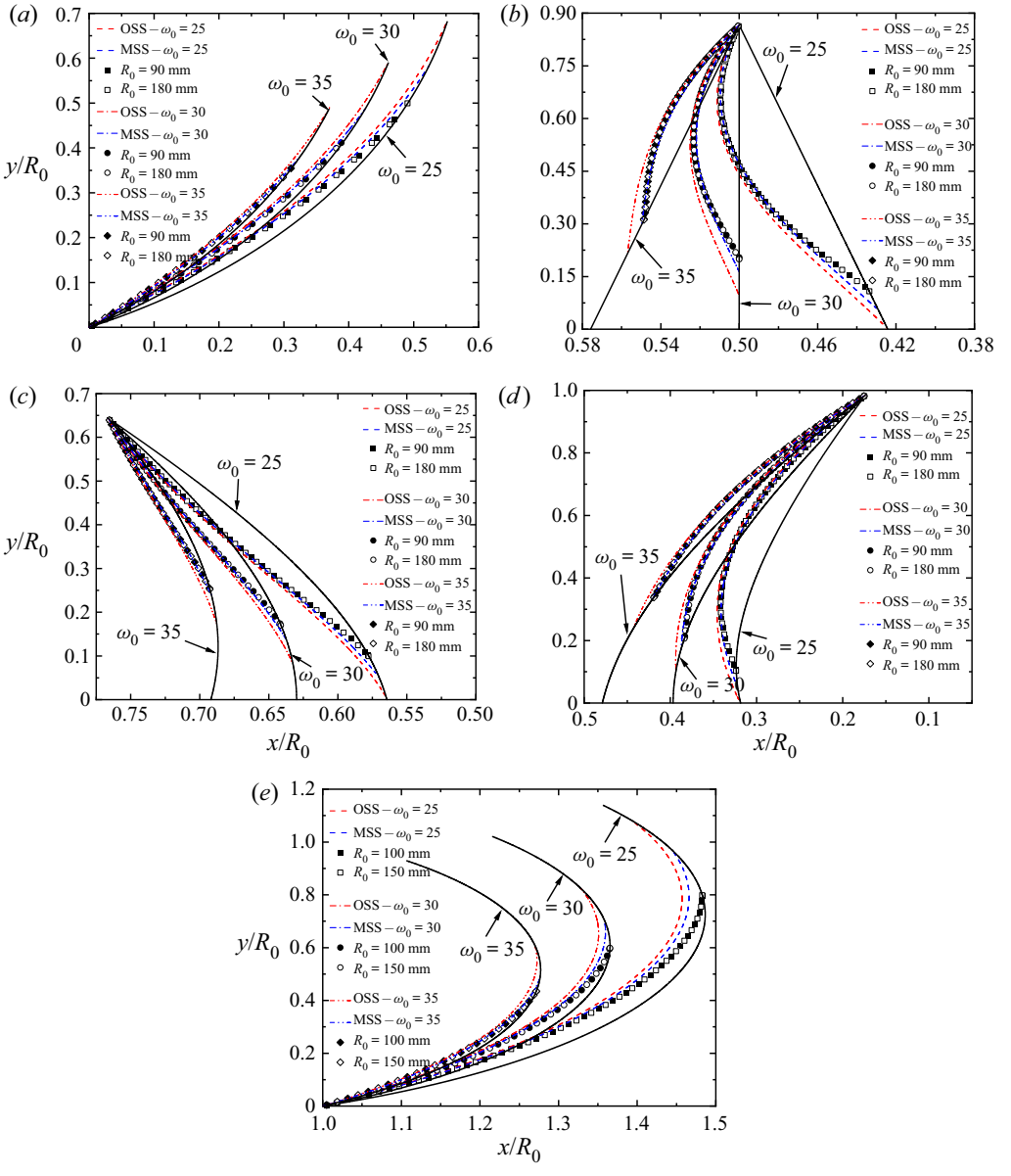


Figure 6. Dimensionless TP trajectories from theoretical and numerical calculations of shock reflections with the wedge angle increased: a planar shock reflection off a concave wedge (*a*), a convergent shock reflection over a straight wedge (*b*), a concave wedge (*c*), a convex wedge (*d*) and a divergent shock reflection over a concave wedge (*e*). The solid lines denote the wedge, and the symbols represent the numerical results. Here OSS and MSS represent the theoretical results calculated by χ^T_{ori} and χ^T_{mod}, respectively, and similarly hereinafter.

TP and the uncertainties of its position (coordinates) are demonstrated in Appendix C. The reflection process of a planar shock over a circular concave wedge, as shown in figure 6(*a*), is similar in cases with different scales, which is consistent with the previous results (Gray & Skews 2017; Koronio *et al.* 2020). It is ascribed to the linear relationship between the geometric scales of the propagation of corner-generated disturbances and

https://doi.org/10.1017/jfm.2022.688 Published online by Cambridge University Press

the TP and the scale of the wedge for reflection. Note that previous experimental works (Takayama & Sasaki 1983; Skews & Kleine 2010) showed that over cylindrical surfaces with different radii, the MR $\rightleftharpoons$ RR transition depended on the Mach strength and the radii of curvature. As the radius of curvature decreases, the deviation between the transition angle in the experiment and the angle predicted by pseudo-steady criterion was increased. They also noticed that when the radius of curvature was considerably increased, the transition occurred very close to the pseudo-steady criterion. However, Hakkaki-Fard & Timofeev (2012) stated that on experimental images the shock and perturbation fronts have a finite optical thickness, which may be significant, especially for high speed movies which typically have lower resolution than still images. This may lead to difficulties in determination of whether or not a particular disturbance has already merged with the reflection point. It may be conjectured that this type of error may be the reason why the catch-up point obtained experimentally by Skews & Kleine (2010) is well ahead (at higher wedge angles) than the theoretical sonic point. In other words, the conclusion obtained by Takayama & Sasaki (1983) and Skews & Kleine (2010) is probably caused by the insufficient spatial and temporal resolutions of experiments, and when the radius of curvature increases, the relative spatial and temporal resolutions would be improved. Also, the discrepancy between the experimental results and inviscid numerical results is related to the existence of viscosity (Kleine *et al.* 2014).

The results in figure 6(*a*) show that the predictions based on χ^T_{mod} and χ^T_{ori} coincide well at the early stages, but deviate from each other quickly from the intermediate to late stages, because the discrepancy between χ^T_{mod} and χ^T_{ori} is proportional to the wedge angle. From the comparison, although the model based on χ^T_{mod} rather than χ^T_{ori} gives a better prediction to the numerical results, an overestimation is still found from the intermediate stages for both of them. This fact shows that the three-shock theory indeed overestimates the χ^T under the conditions considered. In the theoretical calculation, provided that the flow in the TP vicinity adapts to the new boundary conditions immediately when the corner-generated disturbance overtakes it, the new TP trajectory angle is calculated by the wedge angle at the position where the disturbance is generated. For the shock reflection with the wedge angle increased, the corner-generated disturbance is a compression wave, which propagates along the Mach stem and strengthens it. The Mach stem generated when the disturbance overtakes the TP is weaker in intensity relative to the Mach stem generated when an identical shock reflects over a single wedge with the same wedge angle as that at the position where the disturbance is generated (this will be demonstrated in detail in Appendix A). For a given incident shock and wedge angle, the weaker the Mach stem, the smaller the TP trajectory angle. In other words, the TP trajectory angle adopted in theoretical calculations is larger than the actual one, resulting in an overestimation by the theoretical method. In addition, the discrepancy between the numerical and theoretical results would accumulate during the reflection process, which also leads to an overestimation by the theoretical method, especially at the late stages. Besides, some additional factors will result in the difference between the theoretical and numerical results. For example, the accuracy of the three-shock theory in predicting the TP trajectory angle may be inadequate, especially in unsteady shock reflection processes. Also the disturbances caused by the flow diffracting around the curved wedge are not considered in the model, which may affect the movement of the TP. Figures 6(*b*)–6(*d*) show the dimensionless TP trajectories from theoretical and numerical calculations of convergent shock reflection over a straight wedge, a concave wedge and a convex wedge, respectively. Similarly, the reflection process of a convergent shock over a wedge is independent of the scale. Generally, the model can predict the development trend of the TP trajectory.

https://doi.org/10.1017/jfm.2022.688 Published online by Cambridge University Press

The predictions based on χ^T_{mod} and χ^T_{ori} deviate from each other quickly, and the former gives a better prediction. The three-shock theory again obviously overestimates the TP trajectory angle when the Mach stem length starts to reduce from the peak. For each case, the discrepancy between the prediction and the numerical result zooms up as the wedge angle increases. One may also conclude that the model is capable of predicting the TP trajectory when a divergent shock reflects over a concave wedge with the wedge angle increased, as illustrated in figure 6(*e*). For all cases, the model is more accurate for a larger ω_0, probably because there is less accumulation of theoretical error in a shorter reflection process.

Moreover, the MR $\rightarrow$ RR transition wedge angles (ω^t) obtained from the detachment criterion, theoretical calculations (ω^t_t) and numerical simulations (ω^t_n) for all cases are presented in table 2. Here ω^t_t is obtained when the theoretical line intersects with the wedge. For cases with different scales, only a very subtle difference exists between the numerical results, which indicates that the transition angle is independent of the scale. Both ω^t_n and its relative error with ω_d decrease with the increase of ω_0, which is similar to the conclusion obtained in the work of Takayama & Sasaki (1983). The difference in ω^t between the pseudo-steady flow and unsteady flow is caused by the history of the unsteady reflection process, i.e. the accumulation of unsteady effect. The larger the ω_0, the shorter the unsteady reflection process before the MR $\rightarrow$ RR transition occurs, resulting in a smaller difference between ω^t_n and ω_d. In all cases, the relative discrepancy of ω^t between theoretical and numerical results ($|(\omega^t_n - \omega^t_t)/\omega^t_n|$) is smaller when χ^T_{mod} is adopted in a theoretical calculation, and it reduces as ω_0 increases. As a result, the initial wedge angle has an effect on the application of the model. Note that in the theoretical results calculated by χ^T_{ori} when a convergent shock reflects off a convex wedge with $\omega_0 = 25^\circ$, the TP propagating along the ICS ends at the lower boundary instead of the convex wedge, therefore, the MR $\rightarrow$ RR transition wedge angle is absent.

4.2. *Shock reflection with wedge angle decreased*

Now we consider the unsteady shock reflections with the wedge angle decreased, and five different configurations, including a planar shock reflection over a convex wedge, a divergent shock reflection over a convex/straight/concave wedge and a convergent shock reflection over a convex wedge, are investigated. For all cases, three different initial wedge angles ω_0 (50°, 45° and 40°) are adopted to ensure that the MR always occurs over the wedge.

In figure 7 the processes of five types of shock reflection with the wedge angle decreased are shown. In all cases, a MR is generated when the reflection starts, and the Mach stem length continuously increases until the TP meets the wall. Under the conditions considered, the Mach stem is always slightly convexly curved, which should be ascribed to corner-generated rarefaction waves propagating along the Mach stem. Besides, it can be found that a jet is generated around the intersection of the convexly curved slip line with the wedge surface. Such a jet also exists in pseudo-steady shock reflection with the same incident shock Mach number, but it is absent in shock reflection with the wedge angle increased, as discussed above. It seems that the increase of wedge angle inhibits the formation of the jet. Note that for divergent shock reflections with different wedges, as shown in figure 7(*b–d*), there appears hardly any difference qualitatively in the MR configurations, because the curvatures of the convex and concave wedges are limited. As demonstrated in § 3, to provide a relatively straight Mach stem, a wedge angle greater than 20° should always be satisfied during the shock reflection over the wedge. As a

https://doi.org/10.1017/jfm.2022.688 Published online by Cambridge University Press

Shock type	Wedge type	ω_0	R_0	ω_n^t	ω_d	Relative error	ω_{to}^t	Relative error	ω_{tm}^t	Relative error
Planar	Concave	25	100	65.96	50.59	23.3 %	77.13	16.9 %	71.10	7.8 %
		25	150	66.13	50.59	23.5 %	77.13	16.6 %	71.10	7.5 %
		30	100	64.56	50.59	21.6 %	74.06	14.7 %	67.70	4.9 %
		30	150	64.70	50.59	21.8 %	74.06	14.5 %	67.70	4.6 %
		35	100	62.81	50.59	19.5 %	70.73	12.6 %	64.00	1.9 %
		35	150	62.97	50.59	19.7 %	70.73	12.3 %	64.00	1.6 %
Convergent	Straight	25	90	70.76	50.75	28.3 %	84.52	19.5 %	77.70	9.8 %
		25	180	71.10	50.75	28.6 %	84.52	18.9 %	77.70	9.3 %
		30	90	67.83	50.73	25.2 %	78.89	16.3 %	71.74	5.8 %
		30	180	68.22	50.73	25.6 %	78.89	15.6 %	71.74	5.2 %
		35	90	65.06	50.70	22.1 %	73.69	13.3 %	66.22	1.8 %
		35	180	65.42	50.70	22.5 %	73.69	12.7 %	66.22	1.2 %
Convergent	Concave	25	90	70.01	50.72	27.6 %	84.11	20.2 %	77.42	10.6 %
		25	180	70.33	50.72	27.9 %	84.11	19.6 %	77.42	10.1 %
		30	90	67.24	50.69	24.6 %	78.74	17.1 %	71.66	6.6 %
		30	180	67.71	50.69	25.1 %	78.74	16.3 %	71.66	5.8 %
		35	90	64.69	50.67	21.7 %	73.66	13.9 %	66.25	2.4 %
		35	180	64.96	50.67	22.0 %	73.66	13.4 %	66.25	2.0 %
Convergent	Convex	25	90	71.36	50.77	28.9 %	—	—	78.16	9.5 %
		25	180	71.75	50.77	29.3 %	—	—	78.16	8.9 %
		30	90	68.37	50.75	25.8 %	79.27	16.0 %	72.00	5.3 %
		30	180	68.76	50.75	26.2 %	79.27	15.3 %	72.00	4.7 %
		35	90	65.47	50.73	22.5 %	73.93	12.9 %	66.42	1.4 %
		35	180	65.84	50.73	23.0 %	73.93	12.3 %	66.42	0.9 %
Divergent	Concave	25	100	67.34	50.38	25.2 %	81.76	21.4 %	75.76	12.5 %
		25	150	67.50	50.37	25.4 %	81.76	21.1 %	75.76	12.3 %
		30	100	65.42	50.43	22.9 %	77.69	18.8 %	70.99	8.5 %
		30	150	65.54	50.43	23.1 %	77.69	18.5 %	70.99	8.3 %
		35	100	63.24	50.48	20.2 %	73.23	15.8 %	66.03	4.4 %
		35	150	63.37	50.48	20.3 %	73.23	15.6 %	66.03	4.2 %

Table 2. The MR → RR transition wedge angles obtained from detachment criterion, theoretical calculations (ω_t^t) and numerical simulations (ω_n^t) of a shock reflection over a wedge with the wedge angle increased. Here ω_{to}^t and ω_{tm}^t are calculated based on χ_{ori}^T and χ_{mod}^T, respectively, and similarly hereinafter. The unit of angle is degree.

result, the curvatures are limited for the convex and concave wedges, causing similar MR configurations among different cases.

In planar and convergent shock reflections, the reflected shock in the TP vicinity is slightly concavely curved in the early stages and gradually becomes slightly convexly curved in the late stages. As for the three types of divergent shock reflection, the reflected shock in the TP vicinity is always slightly concavely curved. As a result, the divergent shock contributes to making the reflected shock concavely curved.

From the results above, the Mach stem, reflected shock in the TP vicinity and the slip line generally have different shapes or shape variation trends in shock reflections with the wedge angle increased and decreased, which can probably be ascribed to the corner-generated waves or continuously varying boundary conditions that are needed to be satisfied. As mentioned above, all four discontinuities in the TP vicinity are presumed to be straight when the three-shock theory is applied. Therefore, the difference in the shape

https://doi.org/10.1017/jfm.2022.688 Published online by Cambridge University Press

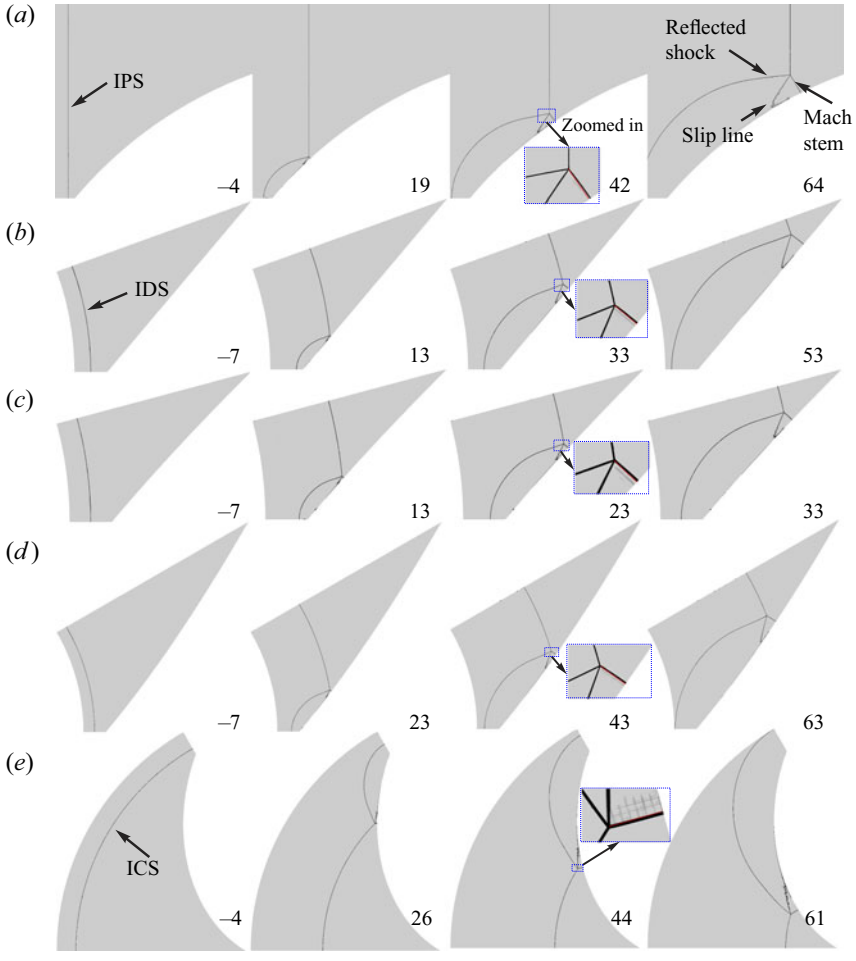


Figure 7. Shock reflection processes with the wedge angle decreased. Planar shock over convex wedge with $\omega_0 = 50^\circ$ and $R_0 = 150$ mm (*a*). Divergent shock over straight wedge (*b*), convex wedge (*c*) and concave wedge (*d*) with $\omega_0 = 50^\circ$ and $R_0 = 100$ mm. Convergent shock over convex wedge with $\omega_0 = 50^\circ$ and $R_0 = 90$ mm (*e*).

or shape variation trend of those discontinuities may cause different performances of the three-shock theory in predicting the TP trajectory angle.

The dimensionless TP trajectories are shown in figure 8 for all cases. The model based on either χ^T_{mod} or χ^T_{ori} underestimates the numerical results for the planar shock reflection over a convex wedge, as shown in figure 8(*a*). It is ascribed to the weaker strength of the Mach stem adopted in the theoretical calculation. The intensity of the Mach stem, when the corner-generated disturbance overtakes the TP, is stronger than that of the Mach stem in the shock reflection over a single wedge using the same shock and wedge angle as those at the position where the disturbance is generated (see Appendix A for details). Besides, the error will be accumulated during the reflection process, which finally results in a relatively large underestimation of numerical results, especially at the late stages. As ω_0 reduces, the discrepancy between the numerical and theoretical results reduces too.

The dimensionless TP trajectories when a divergent shock reflects over a wedge from theoretical and numerical calculations are shown in figures 8(*b*)–8(*d*) for the straight

https://doi.org/10.1017/jfm.2022.688 Published online by Cambridge University Press

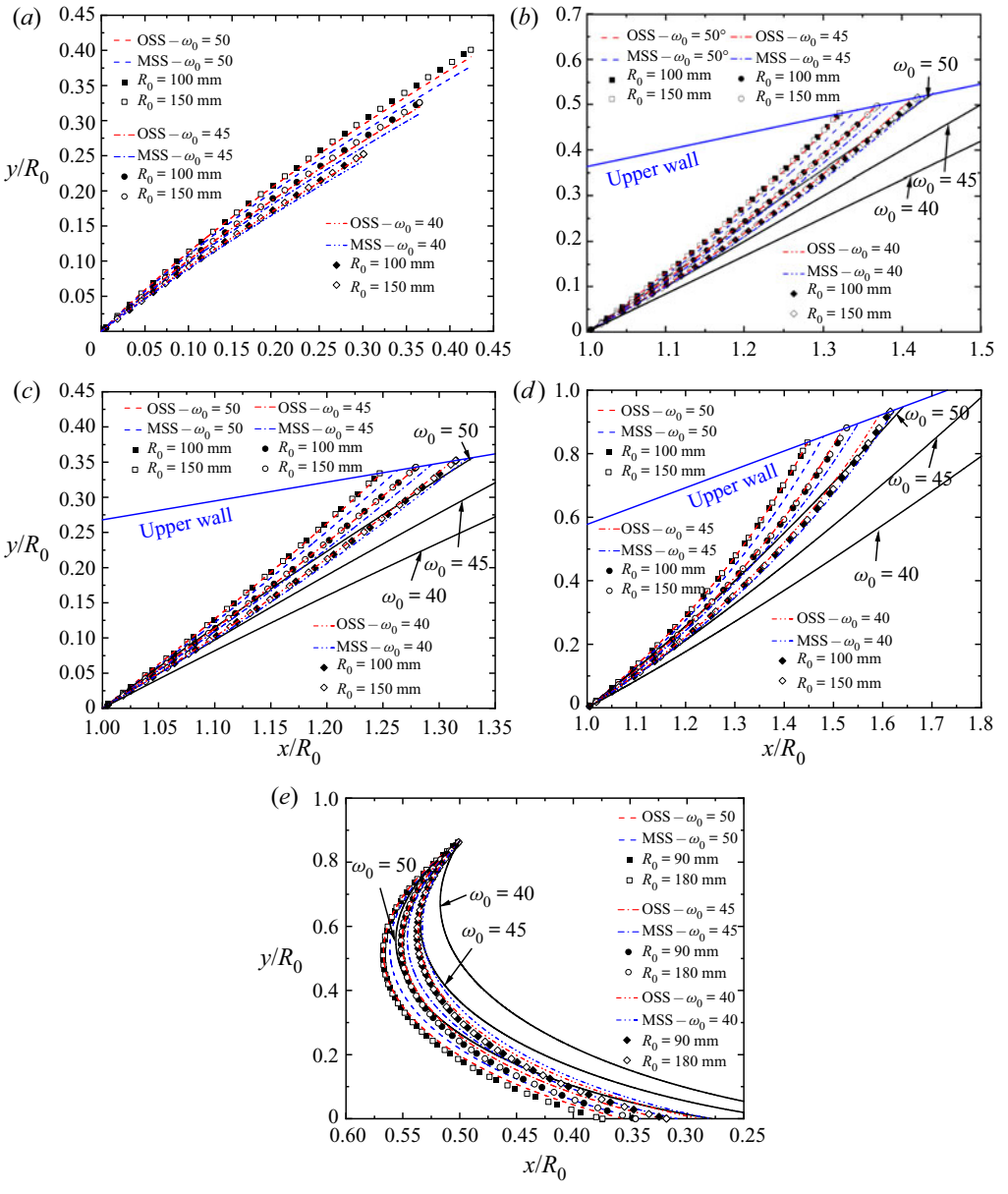


Figure 8. Dimensionless trajectories of the TP from theoretical and numerical calculations of shock reflections with the wedge angle decreased: planar shock reflection over a circular convex wedge (*a*); divergent shock reflection over a straight wedge (*b*), a convex wedge (*c*) and a concave wedge (*d*); convergent shock reflection over a convex wedge (*e*).

wedge, convex wedge and concave wedge, respectively. For cases with the straight/convex wedge, the model based on χ^T_{ori} generally predicts well the TP trajectory, whereas the model based on χ^T_{mod} underestimates the numerical results from the intermediate stages, especially for a larger ω_0. For cases with the concave wedge, the model based on χ^T_{ori} works well for a large ω_0, whereas the model based on χ^T_{mod} works well for a small ω_0. Whether the modification of the prediction by the three-shock theory is necessary or not

https://doi.org/10.1017/jfm.2022.688 Published online by Cambridge University Press

Shock type	Wedge type	ω_0	R_0	$(d/R_0)_n$	$(d/R_0)_{to}$	Relative error	$(d/R_0)_{tm}$	Relative error
Planar	Convex	50	100	0.401	0.391	2.5 %	0.377	5.9 %
		50	150	0.401	0.391	2.6 %	0.377	5.9 %
		45	100	0.326	0.319	1.9 %	0.310	4.9 %
		45	150	0.326	0.319	1.9 %	0.310	4.9 %
		40	100	0.252	0.250	1.0 %	0.243	3.7 %
		40	150	0.253	0.250	1.1 %	0.243	3.8 %
Divergent	Straight	50	100	0.406	0.409	0.7 %	0.430	5.7 %
		50	150	0.407	0.409	0.7 %	0.430	5.7 %
		45	100	0.457	0.455	0.3 %	0.475	4.2 %
		45	150	0.456	0.455	0.3 %	0.475	4.2 %
		40	100	0.511	0.504	1.5 %	0.524	2.4 %
		40	150	0.511	0.504	1.5 %	0.524	2.5 %
Divergent	Convex	50	100	0.291	0.294	0.9 %	0.308	5.7 %
		50	150	0.291	0.294	0.9 %	0.308	5.7 %
		45	100	0.324	0.325	0.3 %	0.339	4.5 %
		45	150	0.325	0.325	0.3 %	0.339	4.5 %
		40	100	0.361	0.358	0.9 %	0.372	2.9 %
		40	150	0.361	0.358	0.8 %	0.372	2.9 %
Divergent	Concave	50	100	0.672	0.672	0.04 %	0.708	5.5 %
		50	150	0.671	0.672	0.1 %	0.708	5.6 %
		45	100	0.763	0.754	1.2 %	0.791	3.6 %
		45	150	0.763	0.754	1.2 %	0.791	3.6 %
		40	100	0.866	0.840	3.0 %	0.877	1.2 %
		40	150	0.865	0.840	2.9 %	0.877	1.3 %
Convergent	Convex	50	90	0.625	0.645	3.1 %	0.659	5.4 %
		50	180	0.625	0.645	3.1 %	0.659	5.4 %
		45	90	0.654	0.679	3.8 %	0.691	5.6 %
		45	180	0.655	0.679	3.8 %	0.691	5.6 %
		40	90	0.682	0.711	4.2 %	0.721	5.7 %
		40	180	0.682	0.711	4.2 %	0.721	5.7 %

Table 3. Dimensionless vertical (radial) displacement of the TP from the leading edge of the wedge to the position where the TP meets the boundary obtained from theoretical and numerical results when a shock reflects over a wedge with the wedge angle reduced.

is dependent on ω_0. The dimensionless TP trajectories when a convergent shock reflects over a convex wedge from theoretical and numerical calculations are shown in figure 8(*e*). The model based on χ^T_{ori} or χ^T_{mod} only predicts well the TP trajectory at the early stages, and underestimates it from the intermediate stages. Relatively, the prediction based on χ^T_{ori} instead of χ^T_{mod} is better.

Moreover, the dimensionless vertical (or radial) displacements of the TP from the leading edge of the wedge to the position where the TP meets the boundary (d/R_0) are compared for numerical and theoretical results. As listed in table 3, generally, the predictions based on χ^T_{ori} instead of χ^T_{mod} are closer to the numerical counterparts, which is contrary to the conclusion in § 4.1. For some specific cases, such as the case of a divergent shock reflecting over a concave wedge with ω_0 of 40°, the prediction based on χ^T_{mod} instead of χ^T_{ori} is closer to the numerical counterpart. As ω_0 reduces, the relative error between numerical results and predictions based on χ^T_{mod} generally reduces except for the case of a convergent shock reflection over a convex wedge, in which the model precision has a weak

https://doi.org/10.1017/jfm.2022.688 Published online by Cambridge University Press

dependency on ω_0. However, the relative error between numerical results and predictions based on χ_{ori}^{T} varies differently as ω_0 reduces. To some extent, the model can predict the TP trajectory when a shock reflects off a wedge with the wedge angle reduced.

5. Conclusions

In this work all known types of 2-D unsteady shock reflections over a single wedge in inviscid perfect air are theoretically and numerically studied, and the emphasis is given to the TP trajectory. By combining Skews' relation and the three-shock theory, which are used to predict the trajectory angles of the corner-generated disturbance and the TP, respectively, and assuming that when the TP is overtaken by corner-generated disturbance, the flow in the vicinity of TP immediately adapts to the new boundary conditions at the position where the disturbance is generated, a model capable of predicting the TP trajectory is established. Then numerical simulations of 2-D unsteady shock reflections over a single wedge are performed. Specifically, five types of shock reflection with the wedge angle increased, including a planar shock reflection off a concave wedge, a convergent cylindrical shock reflection off a straight/concave/convex wedge and a divergent cylindrical shock reflection off a concave wedge; and five types of shock reflection with the wedge angle reduced, including a planar shock reflection off a convex wedge, a divergent cylindrical shock reflection off a straight/convex/concave wedge and a convergent cylindrical shock reflection off a convex wedge, are considered.

For all cases with the wedge angle increased, the Mach stem is always slightly concavely curved, which should be caused by corner-generated compression waves propagating along the Mach stem. The convergent shock contributes to making the reflected shock and the slip line convexly curved. For all cases with the wedge angle decreased, the Mach stem is always slightly convexly curved, which should be ascribed to corner-generated rarefaction waves propagating along the Mach stem. The divergent shock contributes to making the reflected shock concavely curved. The difference in the shape or shape variation trend of those discontinuities may cause different performances of the three-shock theory in predicting the TP trajectory angle. The new model can reasonably predict the TP trajectory in all known types of 2-D unsteady single wedge reflections, and its performance is related not only to the variation trend of the wedge angle, but also to the type of shock and the initial wedge angle. Specifically, for the cases with the wedge angle increased, the model overestimates the TP trajectory if its trajectory angle is calculated by the three-shock theory, but it can provide a better prediction if the TP trajectory angle is modified. For the shock reflection with the wedge angle decreased, on the contrary, the model provides a better prediction if the trajectory angle of the TP is calculated by the three-shock theory. Through the shock-shock/expansion polar analysis, if the corner-generated disturbance is a compression wave (rarefaction wave), the strength of the Mach stem generated when the corner-generated disturbance overtakes the TP is weaker (stronger) in intensity than that of the Mach stem generated when an identical shock reflects over a single wedge which has the same wedge angle as that at the position where the corner-generated disturbance is generated. As a result, the three-shock theory generally overestimates (underestimates) the TP trajectory angle in unsteady reflection with the wedge angle increased (decreased).

Further development of the model can be achieved by modifying the three-shock theory to improve its accuracy in predicting MR with a curved Mach stem, a curved reflected shock and even a curved incident shock, considering the disturbances induced by flow diffraction along the wedge and the effect of unsteady reflection history. However, what we have to face is that each step forward is an enormous challenge.

https://doi.org/10.1017/jfm.2022.688 Published online by Cambridge University Press

Funding. This work was supported by the National Natural Science Foundation of China (Nos. 12022201, 11625211 and 12102425) and Youth Innovation Promotion Association CAS.

Declaration of interests. The authors report no conflict of interest.

Author ORCIDs.
Zhigang Zhai https://orcid.org/0000-0002-0094-5210;
Xisheng Luo https://orcid.org/0000-0002-4303-8290.

Appendix A. Analysis of shock reflection off a double wedge

The model is established based on the assumption that the flow in the vicinity of the TP adapts to the new boundary conditions immediately when the corner-generated upward-travelling disturbance overtakes the TP. In this appendix a planar shock reflection over a double wedge is considered based on the shock dynamics (Whitham 1957; Han & Yin 1993; Xie *et al.* 2005) to discuss the rationality of the assumption. For the reflection of a planar shock over a concave double wedge, if the wedge angle variation is large, the upward-travelling disturbance which carries the information of the sudden variation of the wedge angle is strong (here the strength of the disturbance can be assessed by the variation of the shock Mach number it causes). When the strong disturbance overtakes the TP, an additional downward-travelling disturbance will be generated (Xie *et al.* 2005). The additional disturbance repeatedly propagates and reflects between the TP and the wall, changing the strength and orientation of the Mach stem. As time elapses, the additional disturbance becomes weaker, and the MR over the second wedge approaches the MR of an identical shock over a single wedge with the same wedge angle as the second wedge. In other words, it takes a while for the flow in the vicinity of the newly formed TP to adapt to the new boundary conditions. This process is known as the asymptotic process of the MR over the second wedge (Ben-Dor *et al.* 1988; Xie *et al.* 2005). The assumption adopted in the model indicates that the asymptotic process of the MR over the second wedge is completed instantaneously, i.e. the MR over the second wedge when it is just generated can be regarded as the single wedge reflection. In the following analysis, the rationality of the assumption will be discussed.

The reflection of a planar shock over a concave double wedge, as sketched in figure 9(*a*), is studied. An incident shock with a Mach number of M_0 meets the first wedge with a wedge angle of ω_1, and the MR with the Mach stem 1 is formed over the first wedge. When the Mach stem 1 with a Mach number of M_1 reflects over the second wedge with a wedge angle of ω_2, the Mach stem 2 with a Mach number of M_2 is formed. When the upward-travelling disturbance overtakes the TP, an additional downward-travelling disturbance propagating along the Mach stem 2 is generated, resulting in the formation of the Mach stem 3 with a Mach number of M_3. This shock reflection phenomenon has been investigated by Xie *et al.* (2005) using the shock-shock polar method. According to the shock dynamics (Han & Yin 1993), the shock-shock relation can be expressed as

$$\tan\omega = \frac{M_\omega}{M_i}\frac{\left[1-\left(\dfrac{M_i}{M_\omega}\right)^2\right]^{1/2}\left[1-\left(\dfrac{f(M_\omega)}{f(M_i)}\right)^2\right]^{1/2}}{1+\dfrac{f(M_\omega)}{f(M_i)}\dfrac{M_\omega}{M_i}}, \tag{A1}$$

https://doi.org/10.1017/jfm.2022.688 Published online by Cambridge University Press

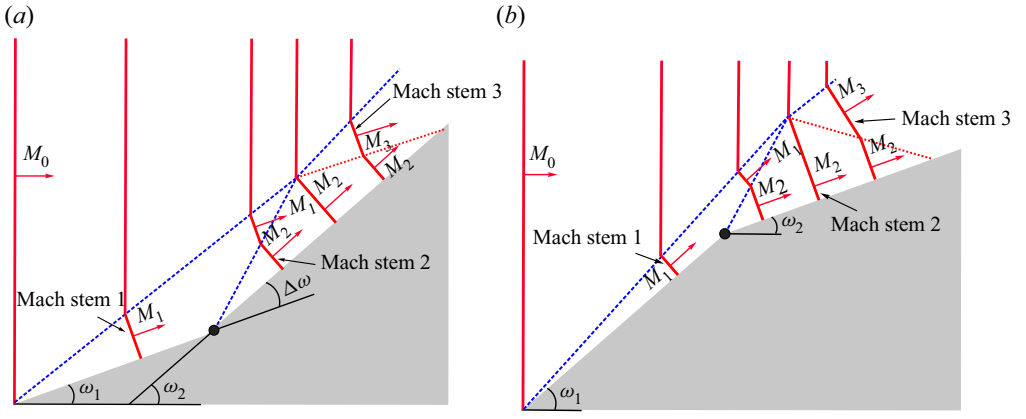


Figure 9. Sketches of a planar shock reflection over a concave (*a*) and convex (*b*) double wedge. Blue dashed lines and red dotted lines represent the trajectories of the upward- and downward-travelling disturbances, respectively.

where ω is the wedge angle, M_i is the initial undisturbed shock Mach number and M_ω is the disturbed shock Mach number, and

$$f(M) = \exp\left[-\int \frac{2M\,\mathrm{d}M}{(M^2-1)K(M)}\right], \tag{A2}$$

where $K(M)$ is a function of M. Then, the shock-shock polaris of the incident shock (I-polar), the Mach stem 1 (M_1-polar) and the Mach stem 2 (M_2-polar) when they serve as the incident shock, respectively, can be obtained by plotting this relation in the (M_ω/M_0)–ω plane.

In this work, M_0 and ω_1 are set as 2.0 and 20°, respectively. It is known that the disturbance intensity is positively correlated with the wedge angle difference ($\Delta\omega = \omega_2 - \omega_1$). To study the effect of the disturbance with different intensities, five different $\Delta\omega$ (20°, 10°, 5°, 1°, 0.1°) are considered. The I-polar, M_1-polar and M_2-polar with different $\Delta\omega$ are plotted in figure 10(*a*). Note that the intersection point of the M_2-polar with the I-polar represents the state (strength and orientation) of the Mach stem 3. Here $M_2 - M_1$ and $M_3 - M_2$ are the shock intensity variations caused by the upward-travelling and downward-travelling disturbances, respectively. As shown in table 4, the downward-travelling disturbance is obviously weaker than the upward-travelling one.

Actually, whether to consider the downward-travelling disturbance or not is equivalent to whether to consider the asymptotic process of the MR over the second wedge or not. This can be measured by comparing M_3 with M_{si} (the Mach number of the Mach stem generated when a planar shock reflects over a single wedge with $\omega = \omega_2$). For this purpose, a parameter $\phi = (M_3 - M_0)/(M_{si} - M_0)$ is introduced. In figure 10(*a*), for the case with $\Delta\omega = 20°$, M_{si}/M_0 and M_3/M_0 are the ordinates of the points denoted by the symbols of a square and circle, respectively. The values of ϕ for cases with different $\Delta\omega$ are shown in table 4. The similarity between the MRs over the second wedge and the single wedge increases as $\Delta\omega$ reduces. When $\Delta\omega = 0.1°$, ϕ approaches 1, which means that the difference between M_3 with M_{si} is very small and the downward-travelling disturbance can be ignored. As we know, the shock reflection off a curved wedge can be regarded as the combination of many double wedge reflections. Therefore, the difference between the shock reflections off a curved wedge and a single straight wedge will accumulate during

https://doi.org/10.1017/jfm.2022.688 Published online by Cambridge University Press

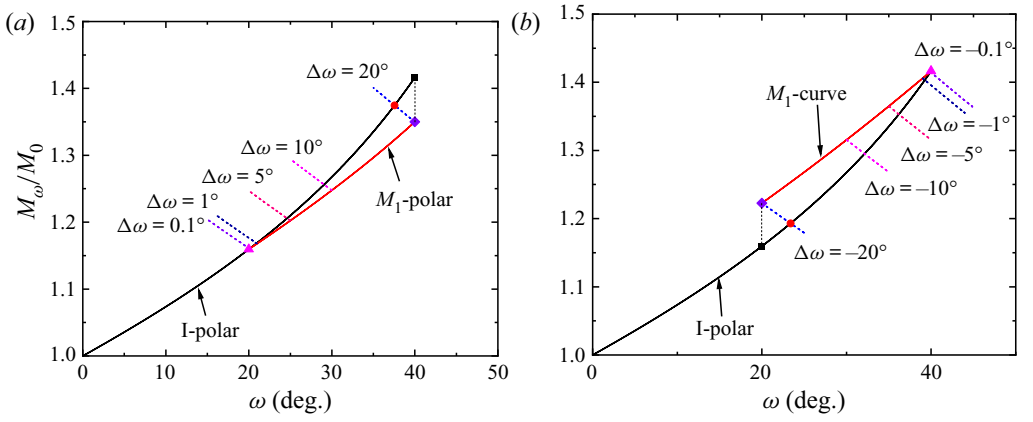


Figure 10. The shock-shock polaris for a planar shock reflection over a concave double wedge with $M_0 = 2.0$ and $\omega_1 = 20°$ (a). The shock-shock polar and shock-expansion curves for a planar shock reflection over a convex double wedge with $M_0 = 2.0$ and $\omega_1 = 40°$ (b). The dashed lines are the shock-shock polaris or shock-expansion curves of the Mach stem 2 when it serves as the incident shock of cases with different $\Delta\omega$.

$\Delta\omega$	M_1/M_0	$M_2 - M_1$	$M_3 - M_2$	$(M_3 - M_2)/(M_2 - M_1)$	M_{si}/M_0	ϕ (ψ)	N	$\phi^N_{0.1}$ ($\psi^N_{-0.1}$)
20°	1.15955	0.38101	0.04926	12.93 %	1.41641	89.98 %	200	92.70 %
10°	1.15955	0.17630	0.01707	9.68 %	1.26767	95.73 %	100	96.28 %
5°	1.15955	0.08559	0.00687	8.03 %	1.20998	98.00 %	50	98.12 %
1°	1.15955	0.01679	0.00113	6.73 %	1.16915	99.62 %	10	99.62 %
0.1°	1.15955	0.00167	0.00011	6.59 %	1.16050	99.96 %	1	99.96 %
−20°	1.41641	−0.38733	−0.05942	15.34 %	1.15955	82.65 %	200	79.87 %
−10°	1.41641	−0.20174	−0.04090	20.27 %	1.26767	90.71 %	100	89.37 %
−5°	1.41641	−0.10297	−0.02377	23.08 %	1.33522	94.95 %	50	94.54 %
−1°	1.41641	−0.02094	−0.00534	25.50 %	1.39884	98.90 %	10	98.88 %
−0.1°	1.41641	−0.00211	−0.00055	26.07 %	1.41462	99.89 %	1	99.89 %

Table 4. The values of M_1/M_0, $M_2 - M_1$, $M_3 - M_2$, $(M_3 - M_2)/(M_2 - M_1)$, M_{si}/M_0, ϕ (ψ) and $\phi^N_{0.1}$ ($\psi^N_{-0.1}$) for cases with different $\Delta\omega$.

the reflection process as the number of double wedge reflections increases. For a rough estimation, it is assumed that the shock reflection over a curved wedge is combined by continuous double wedge reflections with $\Delta\omega = 0.1°$ and $\phi_{0.1}$ (ϕ with $\Delta\omega = 0.1°$) for each double wedge reflection that is the same as that of the first double wedge reflection. For five different $\Delta\omega$ as mentioned above, $N = \Delta\omega/0.1°$ is the number of the double wedge reflection process included. Under the assumptions above and without considering the asymptotic process of the MR over the second wedge, $\phi^N_{0.1}$ can be adopted to estimate the similarity between the final MR over a curved wedge and the MR over a single wedge. The values of $\phi^N_{0.1}$, as given in table 4, are all larger than 92 %. Besides, if the asymptotic process of the MR over the second wedge is considered, the similarity should be higher. Therefore, for the shock reflection with the wedge angle increased, the assumption that the flow in the vicinity of the TP adapts to the new boundary conditions immediately when the weak corner-generated disturbance overtakes the TP is reasonable, especially when the wedge angle variation is limited.

https://doi.org/10.1017/jfm.2022.688 Published online by Cambridge University Press

If the downward-travelling disturbance is also considered, the results will change theoretically. Xie *et al.* (2005) investigated the interaction of two shock-shock disturbances and compared the trajectory angles of the TP with and without considering the downward-travelling disturbance. They found that the discrepancy of the trajectory angles is about 1.5° between the two cases for $M_0 = 2.0$ and $\Delta\omega = 20°$, and, therefore, the downward-travelling disturbance cannot be ignored. In the present work, the upward-travelling and downward-travelling disturbances are much weaker than those considered in the work of Xie *et al.*, and whether the downward-travelling disturbance is considered or not has limited effect on the Mach number of the Mach stem. Because the trajectory angle of the TP is solely related to the Mach number of the Mach stem for a given incident shock Mach number and wedge angle, the trajectory angle of the TP will not change a lot if the downward-travelling disturbance is considered. The effect of a downward-travelling disturbance can be considered in the model if the double wedge reflection is involved. However, in the shock reflection with the wedge angle changing continuously, infinite disturbances would be generated from corners and complicated interactions would occur among different disturbances. This makes an exact analysis of the disturbance propagation and interaction rather difficult.

Then the reflection of a planar shock over a convex double wedge, as sketched in figure 9(*b*), is studied. At the corner, the centred rarefaction waves, represented by a single rarefaction wave in the figure for simplification, are generated. The shock-expansion relation (Han & Yin 1993) can be expressed as

$$\omega = \int_{M_i}^{M_\omega} \left[\frac{2}{(M^2-1)K(M)}\right]^{1/2} \mathrm{d}M. \tag{A3}$$

The shock-shock polar of the incident shock (I-polar), the shock-expansion curve of the Mach stems 1 (M_1-curve) and the shock-expansion curve of the Mach stems 2 (M_2-curve) when they serve as the incident shock, respectively, can be obtained by respectively plotting the shock-shock relation and shock-expansion relation in the (M_ω/M_0)–ω plane. In this work, $M_0 = 2$ and $\omega_1 = 40°$. Similarly, five different $\Delta\omega$ ($-20°$, $-10°$, $-5°$, $-1°$, $-0.1°$) are considered. The I-polar, M_1-curve and M_2-curve with different $\Delta\omega$ are plotted in figure 10(*b*). The point that represents the state of the Mach stem 3 must be on the I-polar, and, therefore, the additional downward-travelling wave generated must be a rarefaction wave. As shown in table 4, similarly, the downward-travelling disturbance can be ignored because the difference between M_3 with M_{si} is very small. For the shock reflection with the wedge angle reduced, a parameter $\psi = 1/\phi = (M_{si} - M_0)/(M_3 - M_0)$ is introduced to characterize the similarity between the MRs over the second wedge and the single wedge. The values of ψ for cases with different $\Delta\omega$ are shown in table 4. Similarly, the assumption that the flow in the vicinity of the TP adapts to the new boundary conditions immediately when the weak corner-generated disturbance overtakes the TP is reasonable. Besides, the shock–shock/expansion polar analysis presented here can also partially explain the model performance for predicting the TP trajectory.

Appendix B. Triple point trajectory equation in divergent shock circumstance

For a divergent cylindrical shock reflection with a constant wedge angle, if the variation of the shock intensity is limited, its effect on the TP trajectory angle is negligible. The TP propagation process for such a divergent cylindrical shock reflection is shown in figure 11.

https://doi.org/10.1017/jfm.2022.688 Published online by Cambridge University Press

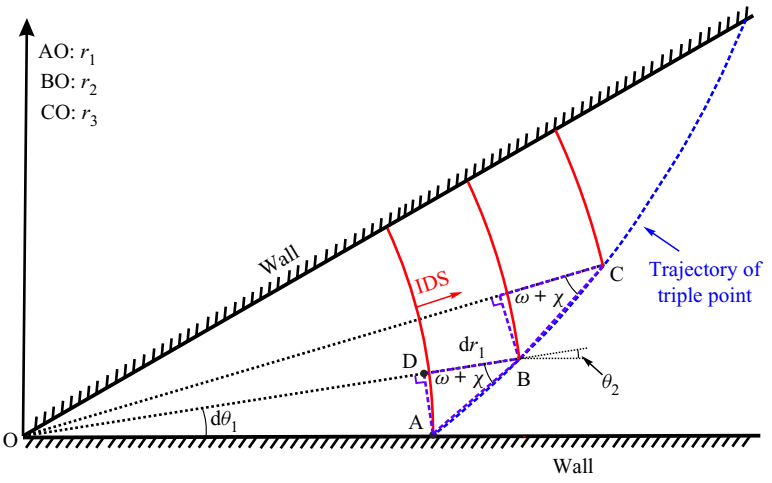


Figure 11. Triple point propagation process in a cylindrical divergent shock reflection with constant wedge angle.

The wedge, reflected shock, Mach stem and slip line are ignored for simplicity. Provided that the wedge angle is ω and the TP trajectory angle is χ, then we have

$$\mathrm{AD} = r_1 \sin(\theta_2 - \theta_1) = r_1 \sin(\mathrm{d}\theta_1) \approx r_1 \,\mathrm{d}\theta_1, \tag{B1}$$

$$\mathrm{d}r_1 = r_2 - r_1 \approx \mathrm{AD} \cot(\omega + \chi) \approx r_1 \cot(\omega + \chi)\,\mathrm{d}\theta_1, \tag{B2}$$

where AD is the distance between points A and D, r_1 and r_2 (θ_1 and θ_2) are the radii (polar angles) of points A and B, respectively, $\mathrm{d}r_1$ and $\mathrm{d}\theta_1$ are the variations of the radius and polar angle of the TP as it moves from point A to point B, respectively. Note that the angle between lines AB and BD is not strictly equal to $\omega + \chi$. However, when $\mathrm{d}\theta_1$ is very small, the deviation between them can be neglected. Since the wedge angle and the TP trajectory angle are constant, the same geometrical relation as (B2) must be satisfied for each part of the TP trajectory. Let the variation of polar angle or radius ($\mathrm{d}\theta$ or $\mathrm{d}r$) be infinitesimal and the TP trajectory can be obtained by integration,

$$\int \frac{1}{r}\,\mathrm{d}r = \int \cot(\omega + \chi)\,\mathrm{d}\theta. \tag{B3}$$

By integration and combining with the initial conditions, we have

$$r = r_1\, \mathrm{e}^{(\theta - \theta_1)\cot(\omega + \chi)}. \tag{B4}$$

Appendix C. Triple point identification

As shown in figure 12, the TP is identified as the intersection point of the incident shock with the reflected shock in the numerical results, a similar method has been adopted in our previous work (Wang *et al.* 2017; Wang & Zhai 2020; Wang *et al.* 2021). Note that whether in planar or cylindrical shock reflections, the incident and reflected shocks are nearly planar in the vicinity of the TP, therefore, this method is applicable to both planar and curved shock reflections. Note that the coordinates of the TP are identified manually. Since the size of the grid in the intersection region of discontinuities is quite small (about 18.8 μm) and the TP should be located within the blue box shown in figure 12, the error of

https://doi.org/10.1017/jfm.2022.688 Published online by Cambridge University Press

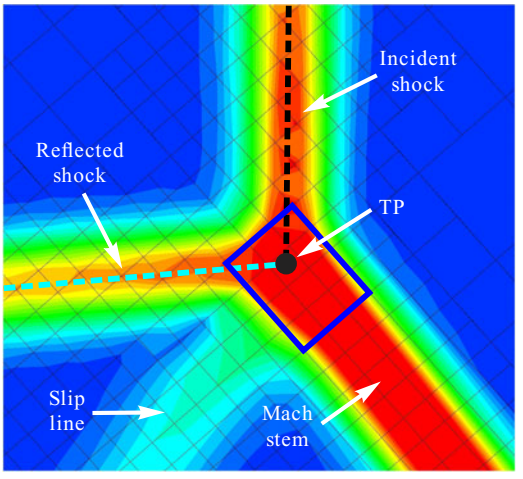


Figure 12. Identification of the TP. The blue box represents the area where the TP may be located.

the manually identified TP coordinates is negligible compared with the scale of the shock reflection process (∼100 mm).

References

Ben-Dor, G. 2007 *Shock Wave Reflection Phenomena*. Springer-Verlag Press.

Ben-Dor, G., Dewey, J.M., McMillin, D.J. & Takayama, K. 1988 Experimental investigation of the asymptotically approached Mach reflection over the second surface in a double wedge reflection. *Exp. Fluids* **6**, 429–434.

Ben-Dor, G., Dewey, J.M. & Takayama, K. 1987 The reflection of a plane shock wave over a double wedge. *J. Fluid Mech.* **176**, 483–520.

Ben-Dor, G. & Takayama, K. 1985 Analytical prediction of the transition from Mach to regular reflection over cylindrical concave wedges. *J. Fluid Mech.* **158**, 365–380.

Bryson, A.E. & Gross, R.W.F. 1961 Diffraction of strong shocks by cones, cylinders, and spheres. *J. Fluid Mech.* **10**, 1–16.

Chester, W. 1954 The quasi-cylindrical shock tube. *Phil. Mag.* **45**, 1293–1301.

Chisnell, R.F. 1957 The motion of a shock wave in a channel, with applications to cylindrical and spherical shock waves. *J. Fluid Mech.* **2**, 286–298.

Cohen, A. & Skews, B. 2020 Very weak shock wave reflection off curved surfaces. *Exp. Fluids* **61**, 174.

Colella, P. & Henderson, L.F. 1990 The von Neumann paradox for the diffraction of weak shock waves. *J. Fluid Mech.* **213**, 71–94.

Dewey, J.M. & McMillin, D.J. 1981 An analysis of the particle trajectories in spherical blast waves reflected from real and ideal surfaces. *Can. J. Phys.* **59**, 1380–1390.

Dewey, J.M. & McMillin, D.J. 1985 Observation and analysis of the Mach reflection of weak uniform plane shock waves. Part 1. Observations. *J. Fluid Mech.* **152**, 49–66.

Dewey, J.M., McMillin, D.J. & Classen, D.F. 1977 Photogrammetry of spherical shocks reflected from real and ideal surfaces. *J. Fluid Mech.* **81**, 701–717.

Geva, M., Ram, O. & Sadot, O. 2018 The regular reflection→Mach reflection transition in unsteady flow over convex surfaces. *J. Fluid Mech.* **837**, 48–79.

Gray, B. & Skews, B. 2017 Reflection of a converging cylindrical shock wave segment by a straight wedge. *Shock Waves* **27**, 551–563.

Gruber, S. & Skews, B. 2013 Weak shock wave reflection from concave surfaces. *Exp. Fluids* **54**, 1571.

Guderley, K.G. 1962 *The Theory of Transonic Flow*. Pergamon Press.

Hakkaki-Fard, A. & Timofeev, E. 2012 On numerical techniques for determination of the sonic point in unsteady inviscid shock reflections. *Intl J. Aerosp. Innovat.* **4**, 41–52.

Han, Z. & Yin, X. 1993 *Shock Dynamics: Fluid Mechanics and its Application*. Kluwer Academic Publishers and Science Press.

https://doi.org/10.1017/jfm.2022.688 Published online by Cambridge University Press

HENDERSON, L.F., VASILEV, E.I., BEN-DOR, G. & ELPERIN, T. 2003 The wall-jetting effect in Mach reflection: theoretical consideration and numerical investigation. *J. Fluid Mech.* **479**, 259–286.

HORNUNG, H. 1986 Regular and Mach reflection of shock waves. *Annu. Rev. Fluid Mech.* **18**, 33–58.

HORNUNG, H.G., OERTEL, H. & SANDEMAN, R.J. 1979 Transition to Mach reflexion of shock waves in steady and pseudo-steady flow with and without relaxation. *J. Fluid Mech.* **90**, 541–560.

HU, T.C.J. & GLASS, I.I. 1986 Blast wave reflection trajectories from a height of burst. *AIAA J.* **24**, 607–610.

ITOH, S., OKAZAKI, N. & ITAYA, M. 1981 On the transition between regular and Mach reflection in truly non-stationary flows. *J. Fluid Mech.* **108**, 383–400.

KLEINE, H., TIMOFEEV, E., HAKKAKI-FARD, A. & SKEWS, B. 2014 The influence of Reynolds number on the triple point trajectories at shock reflection off cylindrical surfaces. *J. Fluid Mech.* **740**, 47–60.

KORONIO, E., BEN-DOR, G., SADOT, O. & GEVA, M. 2020 Similarity in Mach stem evolution and termination in unsteady shock-wave reflection. *J. Fluid Mech.* **902**, A1.

KRASSOVSKAYA, I.V. & BEREZKINA, M.K. 2017 Mechanism of formation of reflection configurations over concave surfaces. *Shock Waves* **27**, 431–439.

LI, H. & BEN-DOR, G. 1999 Interaction of two Mach reflections over concave double wedges-analytical model. *Shock Waves* **9**, 259–268.

LI, M., DING, J., ZHAI, Z., SI, T., LIU, N., HUANG, S. & LUO, X. 2020 On divergent Richtmyer-Meshkov instability of a light/heavy interface. *J. Fluid Mech.* **901**, A38.

LIANG, S.M., HSU, J.L. & WANG, J.S. 2001 Numerical study of cylindrical blast-wave propagation and reflection. *AIAA J.* **39**, 1152–1158.

LIANG, S.M., WANG, J.S. & CHEN, H. 2002 Numerical study of spherical blast-wave propagation and reflection. *Shock Waves* **12**, 59–68.

MACH, E. 1878 Uber den Verlauf von Funkenwellen in der Ebene und im Raume. *Sitz.ber. Akad. Wiss. Wien* **78**, 819–838.

MACLUCAS, D., SKEWS, B. & KLEINE, H. 2020 Shock wave interactions within concave cavities. *Exp. Fluids* **61**, 88.

MILTON, B.E. 1975 Mach reflection using ray-shock theory. *AIAA J.* **13**, 1531–1533.

NDEBELE, B.B. & SKEWS, B.W. 2018 The reflection of cylindrical shock wave segments on cylindrical concave wall segments. *Shock Waves* **28**, 1185–1197.

VON NEUMANN, J. 1943*a* Oblique reflection of shock. *Explos. Res. Rep.* 12. Navy Department, Bureau of Ordinance.

VON NEUMANN, J. 1943*b* Refraction, intersection and reflection of shock waves. *NAVORD Rep.* 203-45. Navy Department, Bureau of Ordinance.

OLIM, M. & DEWEY, J.M. 1992 A revised three-shock solution for the Mach reflection of weak shocks ($1.1 < M_i < 1.5$). *Shock Waves* **2**, 167–176.

SHI, X., ZHU, Y., YANG, J. & LUO, X. 2019 Mach stem deformation in pseudo-steady shock wave reflections. *J. Fluid Mech.* **861**, 407–421.

SKEWS, B.W. 1967 The shape of a diffracting shock wave. *J. Fluid Mech.* **29**, 297–304.

SKEWS, B.W. & ASHWORTH, J.T. 2005 The physical nature of weak shock wave reflection. *J. Fluid Mech.* **542**, 105–114.

SKEWS, B.W. & KLEINE, H. 2007 Flow features resulting from shock wave impact on a cylindrical cavity. *J. Fluid Mech.* **580**, 481–493.

SKEWS, B. & KLEINE, H. 2009 Unsteady flow diagnostics using weak perturbations. *Exp. Fluids* **46**, 65–76.

SKEWS, B.W. & KLEINE, H. 2010 Shock wave interaction with convex circular cylindrical surfaces. *J. Fluid Mech.* **654**, 195–205.

SKEWS, B.W., LI, G. & PATON, R. 2009 Experiments on Guderley Mach reflection. *Shock Waves* **19**, 95–102.

STURTEVANT, B. & KULKARNY, V.A. 1976 The focusing of weak shock waves. *J. Fluid Mech.* **73**, 651–671.

SUN, M. & TAKAYAMA, K. 1999 Conservative smoothing on an adaptive quadrilateral grid. *J. Comput. Phys.* **150**, 143–180.

TAKAYAMA, K. & SASAKI, M. 1983 Effects of radius of curvature and initial angle on the shock transition over concave and convex walls. *Rep. Inst. High-Speed Mech.* **46**, 1–30.

TESDALL, A.M. & HUNTER, J.K. 2002 Self-similar solutions for weak shock reflection. *SIAM J. Appl. Maths* **63**, 42–61.

TESDALL, A.M., SANDERS, R. & KEYFITZ, B.L. 2008 Self-similar solutions for the triple point paradox in gasdynamics. *SIAM J. Appl. Maths* **68**, 1360–1377.

VASIL'EV, E.I. 1999 Four-wave scheme of weak Mach shock wave interaction under the von Neumann paradox conditions. *Fluid Dyn.* **34**, 421–427.

VASIL'EV, E.I., ELPERIN, T. & BEN-DOR, G. 2008 Analytical reconsideration of the von Neumann paradox in the reflection of a shock wave over a wedge. *Phys. Fluids* **20**, 046101.

https://doi.org/10.1017/jfm.2022.688 Published online by Cambridge University Press

VASIL'EV, E.I. & KRAIKO, A.N. 1999 Numerical simulation of weak shock diffraction over a wedge under the von Neumann paradox conditions. *Comput. Maths Math. Phys.* **39**, 1335–1345.

VIERO, D.P., SUSIN, F.M. & DEFINA, A. 2013 A note on weak shock wave reflection. *Shock Waves* **23**, 505–511.

WANG, H. & ZHAI, Z. 2020 On regular reflection to Mach reflection transition in inviscid flow for shock reflection on a convex or straight wedge. *J. Fluid Mech.* **884**, A27.

WANG, H., ZHAI, Z. & LUO, X. 2021 Reflection of a converging shock over a double curved wedge. *Shock Waves* **31**, 439–455.

WANG, H., ZHAI, Z., LUO, X., YANG, J. & LU, X. 2017 A specially curved wedge for eliminating wedge angle effect in unsteady shock reflection. *Phys. Fluids* **29**, 086103.

WHITHAM, G.B. 1957 A new approach to problems of shock dynamics. Part I. Two-dimensional problems. *J. Fluid Mech.* **2**, 145–171.

XIE, P., HAN, Z.Y. & TAKAYAMA, K. 2005 A study of the interaction between two triple points. *Shock Waves* **14**, 29–36.

YUAN, X., ZHOU, J., MI, X. & NG, H.D. 2020 Model for triple-point trajectory of shock reflection over cylindrical concave wedge. *AIAA J.* **58**, 2770–2775.

ZHAI, Z., LIANG, Y., LIU, L., DING, J., LUO, X. & ZOU, L. 2018 Interaction of rippled shock wave with flat fast-slow interface. *Phys. Fluids* **30**, 046104.

ZHAI, Z., OU, J. & DING, J. 2019*a* Coupling effect on shocked double-gas cylinder evolution. *Phys. Fluids* **31**, 096104.

ZHAI, Z., SI, T., LUO, X. & YANG, J. 2011 On the evolution of spherical gas interfaces accelerated by a planar shock wave. *Phys. Fluids* **23**, 084104.

ZHAI, Z., SI, T., LUO, X., YANG, J., LIU, C., TAN, D. & ZOU, L. 2012 Parametric study of cylindrical converging shock waves generated based on shock dynamics theory. *Phys. Fluids* **24**, 026101.

ZHAI, Z., WANG, M., SI, T. & LUO, X. 2014 On the interaction of a planar shock with a light polygonal interface. *J. Fluid Mech.* **757**, 800–816.

ZHAI, Z., ZHANG, F., ZHOU, Z., DING, J. & WEN, C.Y. 2019*b* Numerical study on Rayleigh-Taylor effect on cylindrically converging Richtmyer-Meshkov instability. *Sci. China-Phys. Mech. Astron.* **62**, 124712.

ZHANG, F., SI, T., ZHAI, Z., LUO, X., YANG, J. & LU, X. 2016 Reflection of cylindrical converging shock wave over a plane wedge. *Phys. Fluids* **28**, 086101.

ZHOU, Z., DING, J., ZHAI, Z., CHENG, W. & LUO, X. 2020 Mode coupling in converging Richtmyer-Meshkov instability of dual-mode interface. *Acta Mechanica Sin.* **36**, 356–366.

https://doi.org/10.1017/jfm.2022.688 Published online by Cambridge University Press